

Contents lists available at ScienceDirect

# Journal of Catalysis

journal homepage: www.elsevier.com/locate/jcat



# Aqueous phase hydrodechlorination of trichloroethylene using Pd supported on swellable organically modified silica (SOMS): Effect of support derivatization



Saurabh Ailawar <sup>a</sup>, Anagha Hunoor <sup>a</sup>, Dishari Basu <sup>a</sup>, Benjamin Rudzinski <sup>a</sup>, Laurence Burel <sup>b</sup>, Jean-Marc M. Millet <sup>b</sup>, Jeffrey T. Miller <sup>c</sup>, Paul L. Edmiston <sup>d</sup>, Umit S. Ozkan <sup>a,\*</sup>

- <sup>a</sup> William G. Lowrie Department of Chemical and Biomolecular Engineering, The Ohio State University, 151 W. Woodruff Avenue, Columbus, OH 43210, USA
- <sup>b</sup> Univ Lyon, Université Claude Bernard Lyon 1, CNRS, IRCELYON, F-69626 Villeurbanne, France
- <sup>c</sup>Davidson School of Chemical Engineering, Purdue University, 480 Stadium Mall Drive, West Lafayette, IN 47907-2100, USA
- <sup>d</sup> Department of Chemistry, The College of Wooster, 943 College Mall, Wooster, OH 44691, USA

#### ARTICLE INFO

#### Article history: Received 3 January 2022 Revised 26 April 2022 Accepted 30 April 2022 Available online 06 May 2022

Keywords:
Swellable organically modified silica (SOMS)
Surface derivatization
Palladium
Aqueous phase hydrodechlorination
Pd Leaching
Trichloroethylene
Hydrophobicity
Catalyst deactivation
Organic-inorganic hybrid materials

#### ABSTRACT

Herein, the role of swellability and hydrophobicity of swellable organically modified silica (SOMS) in shielding Pd against deactivation due to HCl produced during hydrodechlorination (HDC) of trichloroethylene (TCE) is investigated. The extent of surface derivatization during sol gel synthesis of SOMS was found to directly impact the extent of hydrophobicity, swellability and surface area, as confirmed by infrared spectroscopy and  $N_2$  physisorption, respectively. Furthermore, after Pd impregnation, the resultant particle size, location, and atomic environment of Pd were also dictated by the extent of support derivatization such that the least derivatized material provided lowest protection to Pd from HCl. Post HCl-treatment, the batch activity rate constants decreased by 66% for the least derivatized sample and 17% for the most derivatized one, suggesting that hydrophobicity and swellability are essential for obtaining high resistance to HCl which could potentially impact the economic viability of HDC of TCE process.

© 2022 Elsevier Inc. All rights reserved.

# 1. Introduction

Swellable organically modified silica (SOMS), a novel catalyst scaffold, belongs to the class of bridged polysilsesquioxanes which are hybrid organic–inorganic materials synthesized by sol–gel technique via co-polymerization of a monomer consisting of an organic group covalently bonded to alkoxysilyl groups. [1–4]. In case of SOMS, bis(trimethoxysilylethyl)benzene (BTEB) is used as the monomer which consists of diethylbenzene (the bridging organic group) which is covalently bonded to two -Si(OCH<sub>3</sub>)<sub>3</sub> groups (two trifunctional silyl groups) [5,6]. The covalent bonds between the Si atoms and the terminal atoms of diethylbenzene are non-hydrolyzable which allows the polymerization to occur only at the methoxy groups attached to the trifunctional Si atoms [1–3]. Owing to the hydrolysis and condensation of the alkoxysi-

lane groups occurring during polymerization, the resulting material often consists of surface silanol groups which are sterically prohibited to condense to Si—O—Si which makes it hydrophilic in nature.

Typically, a silica surface is comprised of isolated, geminal or vicinal silanol groups that are acidic in nature [7,8]. Two major ways of removing or hydrophobizing these groups are thermal treatment and chemical functionalization [7,9,10]. Thermal treatments cause surface dehydration (removal of H-bonded water molecules) followed by dehydroxylation (removal of —OH groups) [7]. This removal of —OH groups from the surface leads to hydrophobization which is why a completely dehydroxylated siloxane surface is hydrophobic [9,10]. Alternatively, chemical modification of the silica surface by replacing —OH groups with long-chained alkyl groups has also been used for surface hydrophobization [7,11]. However, the steric hindrance caused by these long-chained groups does not allow all Si—OH groups to be covered during functionalization. Therefore, a silylating agent with a smaller organic group such as trimethylchlorosilane or

<sup>\*</sup> Corresponding author. E-mail address: ozkan.1@osu.edu (U.S. Ozkan).

similar aminosilane is used to 'end-cap' the residual Si—OH groups and the process is referred to as derivatization [7,11]. For example, silvlation of the surface silanol groups was performed to impart hydrophobicity to Co supported catalysts used for Fischer-Tropsch synthesis and preferential oxidation (PROX) of CO from an H<sub>2</sub>-rich environment [12–15]. The silylation performed on the silica supports for FT synthesis led to a more reducible Co species which resulted in better selectivity of the reaction. Furthermore, the hydrophobization prevented the poisoning of Co sites by water molecules [16,17]. In case of SOMS, derivatization of its surface silanol groups (Si-OH) using hexamethyldisilazane (HMDS) was performed to obtain hydrophobicity [5,6]. Besides being hydrophobic, SOMS is a mesoporous material which can swell to almost 3-4 times its original volume [5,6]. Its application as an absorbent for many organic chemicals has been demonstrated, owing to its high porosity and surface area [18-20].

Our group has investigated the role of SOMS as a support for Pd catalyzed hydrodechlorination of trichloroethylene (HDC of TCE) [21-28] which is an efficient, selective and environmentally friendly route for degradation of TCE [29-34]. TCE, a common industrial solvent [35,36], is a toxic volatile organic contaminant found in groundwater [37–40] and is strictly regulated by US E.P. A. [41,42]. Although Pd catalyzed HDC of TCE is an efficient technique, it suffers from deactivation via leaching (loss of expensive Pd particles) by HCl, an unavoidable by-product [23,32,43,44]. To suppress inhibition by HCl, use of hydrophobic materials to support Pd [45,46], addition of another metal (Fe, Au, Ni) to alter the electronic structure of Pd [47-49] and use of bases such as NaOH or KOH to scavenge the deactivating Cl- ions in the reaction medium have been explored in the literature [50–52]. Our research group has focused on the use of SOMS (a swellable and hydrophobic material) to support and protect Pd [21-26]. In gas phase, Pd/ SOMS was found to be more resistant to deactivation by H<sub>2</sub>O and H<sub>2</sub>S than the commercial Pd/Al<sub>2</sub>O<sub>3</sub> catalyst [21,22,24]. Similarly, in liquid phase, Pd/SOMS showed higher deactivation resistance towards chlorine and sulfur species than Pd/Al<sub>2</sub>O<sub>3</sub> [23-26]. The main aim of this paper is to investigate the cause of high deactivation resistance of SOMS towards HCl (an unavoidable by-product). i.e., to investigate whether the deactivation resistance stems from hydrophobicity or swellability or a combination of these properties of SOMS.

Since  $Al_2O_3$  is neither hydrophobic nor swellable, it cannot be used for comparison with SOMS which is both, hydrophobic and swellable. Therefore, for a better comparison, we synthesized different versions of SOMS using the same precursor (BTEB) such that each of them possessed different combinations of hydrophobicity and swellability. This was achieved by altering the derivatization method used for surface silylation during the synthesis of SOMS. Activity tests and characterization techniques performed with Pd supported on SOMS and its counterparts revealed that not only hydrophobicity but swellability is also essential for high deactivation resistance towards HCl. Such studies which involve the use of animated materials for catalytic applications are quite rarely found in the literature; moreover, those investigating the relationship between the structure of these animated materials and their catalytic performance are even more scarce.

### 2. Experimental

### 2.1. Support synthesis

Synthesis of SOMS was previously reported by Edmiston and co-workers [5,6]. Briefly, SOMS is synthesized using the sol–gel method with bis-(trimethoxysilylethyl)benzene (BTEB) as the precursor dissolved in a suitable water miscible organic solvent (te-

trahydrofuran), followed by addition of water (with 3:1 mol ratio of water:BTEB) containing 0.155 M tetrabutylammonium fluoride as the catalyst. After gelation and ageing for 6 days at room temperature and ambient pressure, the resulting material is broken into 0  $\sim$  0.5 cm pieces while being kept wet with solvent and washed with acetonitrile followed by derivatization of the surface silanol groups with 5% v/v hexamethyldisilazane (HMDS) in acetonitrile for 48 h at 25 °C. The gel is then rinsed to remove excess HMDS, dried at room temperature followed by grinding in a ball mill at 200 rpm. The ground particles were sieved to obtain a particle size of less than 74  $\mu$ m. This particle size was chosen to ensure absence of internal mass transfer limitations [23].

Multiple batches were synthesized and mixed prior to impregnation. Following the same method, another sample was synthesized wherein no derivatization was performed after washing with acetonitrile. This sample was named as SOMS-UD where UD stands for un-derivatized. The third type of support material was synthesized by drying the sample for 48 h after washing it with acetonitrile and then derivatizing with HMDS. This sample was named as SOMS-PDD (PDD: post-drying derivatized).

#### 2.2. Impregnation of Pd on support

Supported Pd catalysts with ~ 1.25% (w/w) Pd loading (hereafter written as Pd/SOMS or Pd/SOMS-UD or Pd/SOMS-PDD for brevity) were synthesized using incipient wetness impregnation (IWI) technique wherein, a solution of 10.6 mg Pd(II) acetate (Sigma-Aldrich, 99.9%) in 8 mL acetone was added dropwise to a thin layer of ground 1 g support particles. Intermittent drying of the support was carried out to remove excess acetone, at room temperature. After the entire solution was taken up by the support, it was dried overnight at room temperature. For reduction, a 0.05 g of NaBH<sub>4</sub> was dissolved in 15 mL of 95% (v/v) ethanol-water solution. The quantity of NaBH4 was added in excess to ensure complete reduction of Pd acetate. This solution was slowly added to the unreduced catalyst powder and a color change from pale orange to black was observed. Post reduction, the catalyst was filtered using a Whatman filter paper with 11 um pore size and washed several times with ethanol to get rid of residual impurities. The catalyst was dried at 60 °C, overnight prior to use. This method was used to support Pd on all three support materials reported in

Lastly, Pd content of the synthesized samples was verified using inductively coupled plasma mass-spectrometry (ICP-MS). Powdered sample weighing 0.05 g was digested with 5 mL concentrated ultrapure HNO3, 3 mL HCl, 2 mL HF at 220 °C to achieve complete digestion. Samples were diluted to 100 mL and then an aliquot was diluted an additional 50 times for analysis. Quantitative measurements were performed on a Perkin-Elmer Sciex Elan DRCii Inductively Coupled Plasma Dynamic Reaction Cell Mass Spectrometer. Standards for calibration were prepared using commercial Pd stock solution and 3 replicates were analyzed for each sample and standard. Additionally, no detectable Pd was found in the filtrate obtained after washing the sample several times with ethanol.

# 2.3. Fourier transform infrared spectroscopy (FTIR)

Sample weighing 200 mg was mixed with KBr in the (w/w) ratio 1:10 to form self-supporting pellets. These pellets were mounted on a sample holder of a Thermo Scientific 6700 Nicolet FTIR Transmission IR cell which is equipped with a KBr beam splitter and a liquid  $N_2$ -cooled MCT-A. A Michelson interferometer was used to collect Fourier transformed IR spectra within a range of  $600~\text{cm}^{-1}$  to  $4000~\text{cm}^{-1}$ . The cell environment was purged with  $N_2$  to minimize the presence of other gases. OMNIC 8.1 software was used

to determine and assign peak positions while analyzing the collected spectra. Data was collected on two batches of each sample using KBr as background.

## 2.4. N<sub>2</sub> Physisorption

 $N_2$  physisorption was used to determine the textural properties of the catalysts with an accelerated surface area and porosimetry instrument (ASAP 2020) by Micromeritics. Catalyst powder weighing 100 mg was degassed overnight at 120 °C, followed by cooling at 77 K and dosing  $N_2$ . Once saturated with  $N_2$ , the material was degassed again to remove the physisorbed  $N_2$ . The surface area was determined using Brunauer-Emmett-Teller (BET) method within 0.06–0.2 times the relative pressure [53]. The desorption branch of the isotherm was used to obtain the pore size distribution and pore volume by Barrett-Joyner-Halenda (BJH) method [54]. Data was collected using singular approach. It should be noted that SOMS is a thermally stable up to 400 °C [15] and hence, degassing at 120 °C is considered to cause no structural alteration.

### 2.5. Transmission electron microscopy (TEM)

TEM images were obtained on a Jeol 2010 LaB6 microscope operating at 200 kV. The samples were prepared by mixing the catalyst powder with ethanol followed by dispersing this slurry on standard holey carbon-covered copper TEM grids. The particle size distribution analysis was made using FIJI, an open-source platform for biological-image analysis [55]. Data was collected using singular approach.

#### 2.6. Ex-situ treatment with HCl

To investigate the interaction of HCl, the unavoidable HDC product, with Pd, the pristine catalysts were soaked in an aqueous solution of HCl. Due to the reversible nature of adsorption of HCl with Pd particles, ex-situ treatment was found to be a valid methodology to test catalyst's deactivation tolerance [23,28]. Organics such as ethanol or TCE were added to the aqueous HCl solution for determining their influence on the interaction of HCl and Pd. No H2 was used to avoid the occurrence of HDC reaction during soaking experiments. A catalyst amount of 0.35 g was stirred in a 300 mL aqueous solution of 0.35 M HCl and 1000 mg/L of TCE or 10% (v/v) ethanol, in a 0.5 L three-necked flask. The concentration of organics was chosen to mimic those in the feed. Prior to adding the catalyst, the flask was flushed with inert gas and the soaking was performed at ambient pressure and room temperature. The concentration of HCl was chosen based on the total HCl concentration produced during the HDC reaction conducted in batch reactor if complete conversion of TCE was obtained. The slurry was filtered post soaking, and the catalyst was thoroughly rinsed with D.I. water. The filtered solid was dried overnight at 110 °C.

# 2.7. Inductively coupled plasma-mass spectrometry (ICP-MS)

Elemental analysis of the HCl solution collected after chloride treatment of the catalysts was performed to determine the extent of leached Pd. The HCl solutions were filtered and diluted 10 times with a 10% v/v ultrapure aqua regia prior to analysis. Solutions with Pd concentrations of 0, 10, 50, 100, 200, 500  $\mu$ g/L were used as standards. Samples were measured on a ThermoFinnigan Element2 ICP-SFMS at resolution (R) = 300. 5 isotopes of Pd ( $^{104}$ Pd,  $^{106}$ Pd,  $^{106}$ Pd,  $^{108}$ Pd,  $^{110}$ Pd) were analyzed and averaged, all isotopes agreed well.

#### 2.8. CO pulsing using mass spectrometry

Catalyst weighing 50 mg was packed in a quartz glass reactor (0.5 in. ID) fitted with a frit to support the catalyst. The packed reactor was placed in a Carbolite MTF 10/15/130 furnace and was treated under He, at  $110~{}^{\circ}\text{C}$  for 1 h to remove physisorbed moisture,  $\text{CO}_2$ , and other loosely bound impurities. Post heattreatment, the temperature was lowered to  $40~{}^{\circ}\text{C}$ . During adsorption, pulses of 3% CO/He gas was passed through a six-port valve assembly consisting of a  $100~{}^{\circ}\text{L}$  sample loop and the exit CO (m/z=28~signal) was detected using an MKS Cirrus II mass spectrometer operated in scanning ion mode.

# 2.9. X-ray photoelectron spectroscopy (XPS)

Surface analysis of the synthesized and HCl soaked catalysts was performed by XPS using a Kratos Axis Ultra instrument operated under ultra-high vacuum (UHV) i.e.,  $10^{-9}$  torr. The X-rays were generated from a monochromated Al K  $\propto$  source (12 kV, 10 mA). The samples were loaded on carbon tape and outgassed under UHV overnight and a charge neutralizer (2.1 A, 1.3 V) was used while collecting spectra. Survey spectra were collected in the range 1200–0 eV and the high-resolution scans of O1s, Pd 3d, C1s, Cl2p and Si2p regions were collected with 16 sweeps and varied dwell times. C1s peak at 284.5 eV was used for internal calibration. Data was collected using singular approach and analyzed using CasaXPS software.

# 2.10. Extended X-ray absorption near edge structure (EXAFS)

EXAFS experiments were performed at the insertion device (ID) beamline of the Materials and Research Collaborative Access Team (MRCAT), sector 10 of the Advanced Photon Source, Argonne National Laboratory [56]. While collecting transmission data of pelletized samples supported in a 'six-shooter', a cryogenically cooled Si(111) monochromator with a Pt coated mirror was used for harmonics rejection. A hole-width of 0.12 cm<sup>2</sup> with  $\sim 500$  mg gave an edge step ( $\Delta ux$ ) of 0.5 for the Pd/SOMS samples and 1.6 for the Pd foil (used for energy calibration). Data was collected using singular approach and analyzed was performed using WIN-XAS97 software following the standard procedure [57]. First derivative spectra were used to determine the threshold energy of the calibrated samples. Least square fits in R-space and kspace of the isolated nearest neighbor were used to determine EXAFS parameters such as the coordination number (CN) and interatomic bond distance (R). References such as Pd(II)chloride and Pd foil were used for obtaining phase shifts and backscattering amplitudes. For fitting purpose, CN and R associated with Pd-Cl scattering in Pd(II)chloride was 4 and 2.31 Å, respectively whereas, with Pd-Pd scattering in foil were fixed at 12 and 2.75 Å, respectively.

# 2.11. Catalytic activity experiments

Batch reactions were performed at 30 °C and 50 bar, using a 300 mL 4560 mini-benchtop stirred reactor from Parr Instruments Co. equipped with 4848-controller (PID) for temperature and stirring speed. A 200 mL feed solution consisting of 1000 mg/L of TCE, and 450 mg/L of tetrahydrofuran (THF) dissolved in water was added to the reactor vessel. Losses occurring due to volatilization of TCE were accounted for by noting the losses in THF (internal standard) concentration. Furthermore, the low THF concentration and its high solubility in water does not allow any significant absorption of THF in SOMS thereby avoiding any swelling of SOMS by THF. Prior to reaction, pure He, at 30 mL/min for 30 min was bubbled through the solution to remove dissolved gases. The reac-

tor was pressurized in two steps. Initially, 45 bar of pure  $H_2$  was introduced into the reactor and a sample ( $\sim$ 1 mL) was drawn out from the liquid phase to obtain the initial concentration of TCE (time = 0 sample) which was reduced to 250 mg/L. As soon as the initial sample was collected, the total pressure of the reactor was raised to 50 bar by introducing  $H_2$  through a customized catalyst addition device (CAD) and the reaction was started. CAD is an internal Teflon-sealed chamber holding 5 mg of powdered catalyst. As the reaction progressed, liquid phase samples ( $\sim$ 1mL) were collected at intervals of 40 min (total reaction time 240 min) in a sealed vial fitted with a rubber septum. These samples were shaken and allowed to equilibrate prior to injecting them into the HPLC. Reaction runs were validated by running reference reaction before and after a test sample. The error in measurement was less than 5%.

The concentration of the organic educts was determined using high-performance liquid chromatography (HPLC). During the operation, the solvents (water and acetonitrile, Sigma Aldrich, HPLC grade) were pumped using a gradient mode with a starting 95:5 (v/v) ratio of acetonitrile:water changed to 50:50 (v/v) over 38 min. A C18 column obtained from Grace Alltima was operated in reverse phase and used for separation of compounds. Finally, a UV-vis detector obtained from Shimadzu (SPD-20A) with a D2 lamp, and a dual-chamber mode (220/200 nm) was used for compound detection.

For this experimental set up, impellor speed is maintained at 1700 rpm to avoid external mass transfer limitations [23]. Furthermore, internal mass transfer limitations do not exist in presence of 10% ethanol as shown by the use of Madon-Boudart criterion in our previous study [28].

# 3. Results and discussion

# 3.1. Fourier transform infrared spectroscopy (FTIR)

FTIR spectroscopy was used to determine the structural changes occurring in SOMS caused by derivatization of the surface silanol groups. These FTIR spectra were collected in transmission mode and were divided in three regions: low-frequency (650–1250 cm<sup>-1</sup>), mid-frequency (1250–1700 cm<sup>-1</sup>) and high-frequency (1700–4000 cm<sup>-1</sup>), shown in Fig. 1a, b and c respectively.

# 3.1.1. Groups originating from BTEB (precursor)

All spectra show several similar bands due to functional groups common to all three samples. For example, bands at 694 cm<sup>-1</sup> in the low frequency region can be assigned to out of plane C-H bending vibrations associated with mono- and *meta*-substituted benzene rings [58], while bands in the mid-frequency region, 1407 to 1606 cm<sup>-1</sup> can be assigned to in-plane bending vibration modes of the mono- and *meta*-substituted benzene rings [58]. These peaks belong to aryl groups originating from BTEB, have similar relative intensities in all three samples indicating that their concentration is similar in all three samples. Another set of bands, having similar positions and relative intensities across all samples were 2858–2863 cm<sup>-1</sup> and 2931–2933 cm<sup>-1</sup> belonging to symmetric and asymmetric stretching, respectively, of the C-H bonds in methylene group arising from BTEB [58–60].

# 3.1.2. Groups formed by derivatization with HMDS

The spectral differences among the three samples arise due to differences in their extent of derivatization. For example, peaks

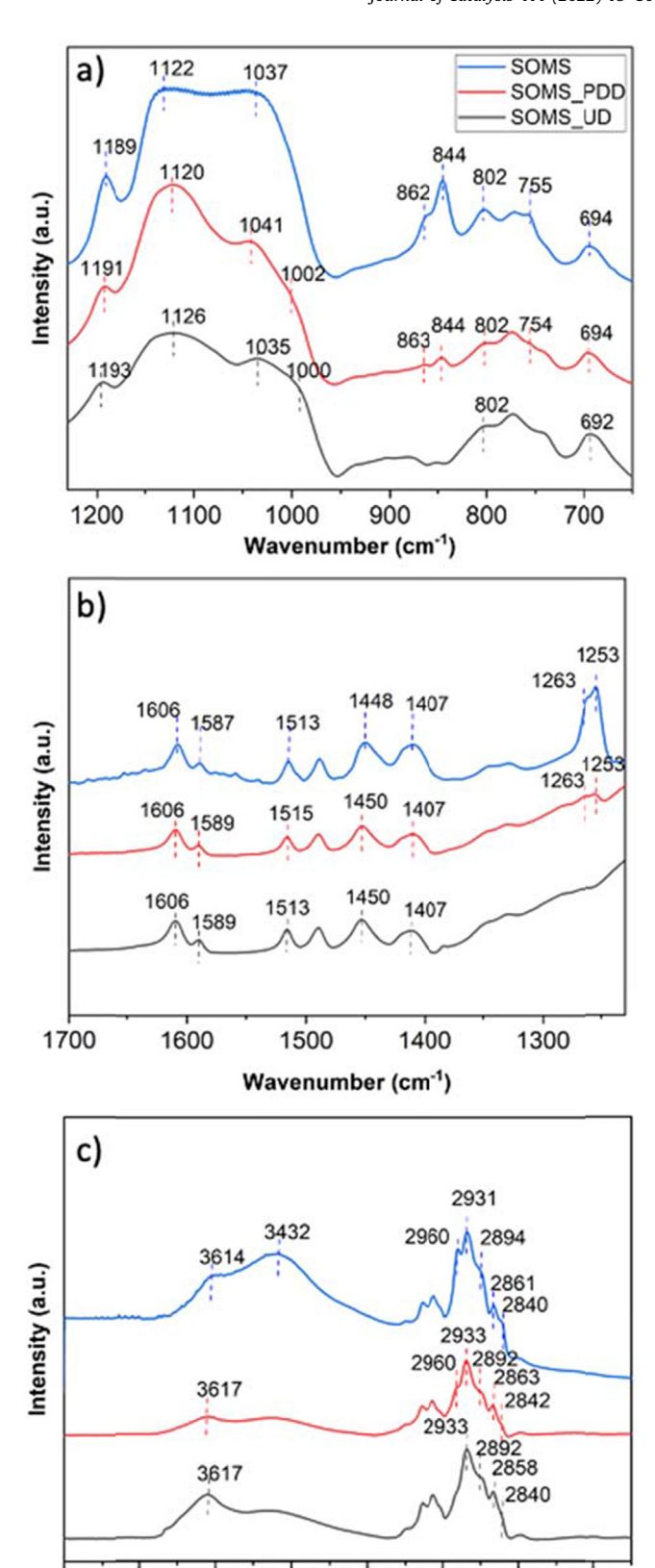


**Fig. 1.** Transmission IR spectra of structurally altered SOMS samples in the (a) low-, (b) mid- and (c) high-frequency region.

3200

Wavenumber (cm<sup>-1</sup>)

3000

2800

2600

3400

4000

3800

3600

S. Ailawar, A. Hunoor, D. Basu et al. Journal of Catalysis 411 (2022) 15–30

observed at 755, 802, 844, 862 cm<sup>-1</sup> (Fig. 1a); 1253, 1263 cm<sup>-1</sup> (Fig. 1b); 2960 and 2892-2984 cm<sup>-1</sup> (Fig. 1c) were present in SOMS and SOMS-PDD samples but absent in SOMS-UD, indicating that these peaks belong to -Si-(CH<sub>3</sub>)<sub>3</sub> groups formed only as a result of derivatization. Among these peaks, 755, 802, 844, and 862 cm<sup>-1</sup> (low-frequency region) could be assigned to rocking vibrations of Si-CH<sub>3</sub> groups [61-64]; peaks at 1253 cm<sup>-1</sup> and 1263 cm<sup>-1</sup> (mid-frequency region) could be attributed to symmetric deformation of Si-C bonds [65] and, peaks at 2960 cm<sup>-1</sup> and 2892-2984 cm<sup>-1</sup> (high-frequency region) can be ascribed to the asymmetric and symmetric stretching of CH<sub>3</sub> groups bound to Si atoms, respectively [58,60,66]. Although SOMS and SOMS-PDD showed similarity peak positions, their relative intensities were different. This is because, silanol groups on the gel decrease after drying due to condensation. However, SOMS being derivatized prior to drying, it has abundant (non-condensed) silanol groups available for derivatization. In contrast, the SOMS-PDD is derivatized after drying during which, most of the silanol groups might have already condensed. This difference in concentration of silanol groups available for derivatization in case of SOMS and SOMS-PDD, eventually results in different concentration of -Si-(CH<sub>3</sub>)<sub>3</sub> groups present on the final samples.

Furthermore, the peaks corresponding to 1189–1193 cm<sup>-1</sup> and 2840–2842 cm<sup>-1</sup> can be attributed to rocking and stretching vibrations of C-H bonds in Si-OCH<sub>3</sub>, respectively [64,67–70], which originate from BTEB. SOMS displayed high concentrations of Si-CH<sub>3</sub> and Si-OCH<sub>3</sub> groups implying that derivatization of Si-OH groups imparts hydrophobicity to the matrix while preventing the condensation of Si-OCH<sub>3</sub> groups. On the other hand, SOMS-UD being underivatized, Si-OH was dominant on that sample, as shown by high intensities of peaks at 1000 cm<sup>-1</sup> and 3614 cm<sup>-1</sup> [25,71–73].

Finally, the band at 3432 cm<sup>-1</sup> was assigned to H-bonded OH groups of loosely bound ambient moisture [25,71], as it disappeared after heating the sample at 110 °C under He (shown in Fig. S1). In summary, SOMS-UD predominantly comprised of hydrophilic Si-OH groups, whereas SOMS and SOMS-PDD comprised of the hydrophobic Si-CH<sub>3</sub> groups. Visual evidence of this difference in hydrophobicity was also obtained by mixing these powders in water as shown in Fig. 2. SOMS-UD is dispersed to a

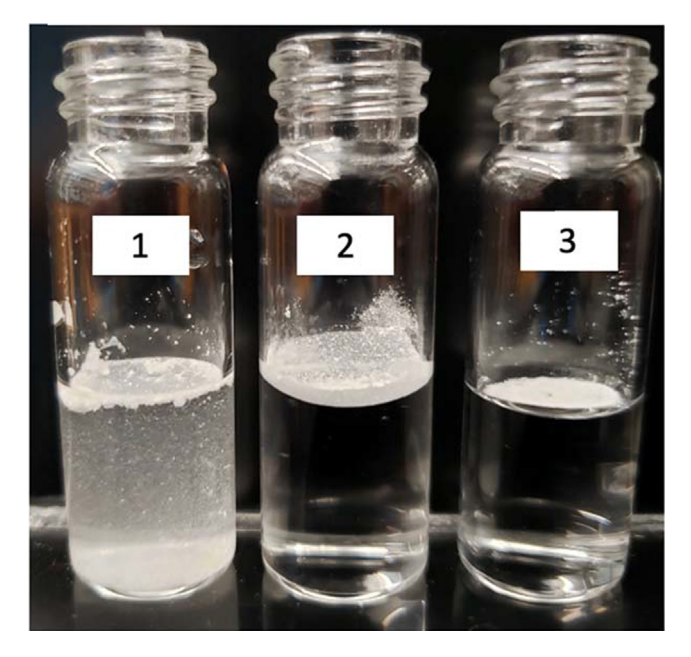


**Fig. 2.** Visual representation of hydrophobicity of 1) SOMS-UD; 2) SOMS-PDD; 3) SOMS.

higher extent in water whereas, SOMS and SOMS-PDD (the derivatized samples) could not be dispersed as easily.

#### 3.1.3. Si-O-Si linkages

In case of Si-O-Si groups, a broad peak was observed in the lowfrequency region of the spectra (1120 to 1040 cm<sup>-1</sup>). Pure silica, with an ordered arrangement of Si-O-Si bonds with similar bond angles ( $\theta$  = 144) exhibits a Gaussian shaped IR absorption peak which is often broadened due to random arrangement of Si-O-Si bonds [74]. In case of SOMS, SOMS-UD and SOMS-PDD, two regions were formed containing these broadened Si-O-Si peaks with different relative intensities (Fig. 1a). The peaks around 1120 cm<sup>-1</sup> and 1037 cm<sup>-1</sup> can be assigned to the asymmetric stretching of the linearly (bond angle  $\sim 180^\circ)$  and obliquely (bond angle between  $120^\circ$ to 130°) bonded Si-O-Si [59,63,66,75-77]. Materials with higher concentration of low bond angle Si-O-Si species (1037 cm<sup>-1</sup>) relative to the linearly bonded Si-O-Si species are more flexible [76]. In Fig. 1a. the relative intensity of the strained Si-O-Si bond peak decreases in the order: SOMS > SOMS-PDD > SOMS-UD, thereby implying that flexibility decreases in that order. This can be further supported by results reported in our previous study wherein thermal treatment of SOMS (at 600 °C), was found to cause a loss in swellability accompanied by a decrease in the intensity of the low-angle Si-O-Si species relative to the linear ones [18,21]. Thus, it can be concluded that swellability of the materials in this study decreases in the order: SOMS > SOMS-PDD > SOMS-UD.

## 3.2. N<sub>2</sub> Physisorption

N<sub>2</sub> physisorption was performed to determine the textural properties of SOMS, SOMS-UD and SOMS-PDD and the results are shown in Table 1. In general, all the samples were found to possess high surface areas probably due to the presence of organic groups (such as the aryl group) in their structure [1,2]. The BET surface areas of SOMS and SOMS-PDD were similar but that of SOMS-UD was slightly lower, possibly due to lack of derivatization. This is consistent with the observations made by Mariscal et al., who reported that silvlated (derivatized) titania-silica xerogels possessed higher BET surface area as compared to their non-silvlated counterpart [78]. As reported by Celik et al., the surface area and pore size obtained from N<sub>2</sub> physisorption may not be the true values as the material is in its shrunken form during the physisorption process [26]. After swelling it is expected that the values of these textural properties (surface area and pore sizes) will increase because it is only conceivable that volumetric expansion due to swelling will increase the surface area and pore size. However, characterizing these materials in their dry form under identical conditions revealed differences that are discussed below.

Table 1 also reports the C value (also known as the BET constant) of the support material, which is typically used to gauge the strength of interaction of the adsorbent with the adsorbate [12,15,78]. Magnitude of C value is directly proportional to the strength of  $N_2$  adsorption and inversely proportional to surface hydrophobicity [12,78]. Table 1 shows that both SOMS and SOMS-PDD have significantly smaller C values than SOMS-UD indicating its low surface hydrophobicity. These findings are consistent

**Table 1**Textural properties of SOMS, SOMS-UD and SOMS-PDD.

Samples	BET Surface Area C valu (m²/g)		e* BJH Pore size (nm)	
SOMS	546	58	4.6	
SOMS-UD	458	151	2.5	
SOMS-PDD	574	88	3.0	

<sup>\*</sup> C value refers to the BET constant.

with the FTIR results which showed that the surfaces of SOMS and SOMS-PDD, consist of 'hydrophobic' Si—(CH<sub>3</sub>)<sub>3</sub> groups, whereas that of SOMS-UD mainly consists of 'hydrophilic' Si—OH groups.

Lastly, the average pore size calculated by BJH method applied during desorption of  $N_2$  (Table 1) show that, although, all samples have mesopores as per IUPAC [79], SOMS-UD has smaller pores than the other samples. Due to lack of derivatization of the silanol groups, SOMS-UD undergoes more cross-linking than its derivatized counterparts which may result in its smaller pore-size [80]. Furthermore, SOMS-PDD possessed smaller pore size than SOMS which could be due to its derivatization being performed after drying the gel (as opposed to SOMS where it is performed prior to drying), causing more crosslinking than SOMS. In summary, it can be said that the sequence of derivatization during support synthesis is an important factor affecting their textural properties.

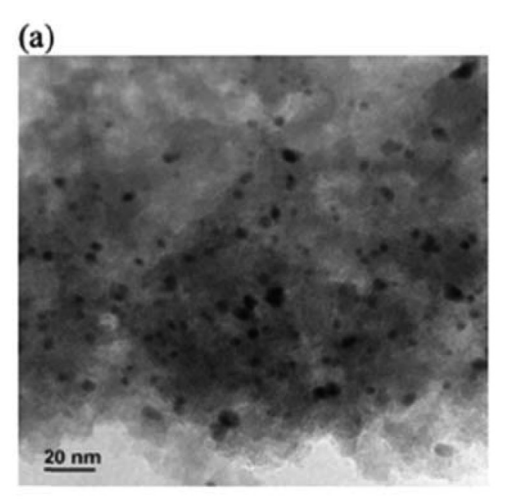
#### 3.3. Transmission electron microscopy (TEM)

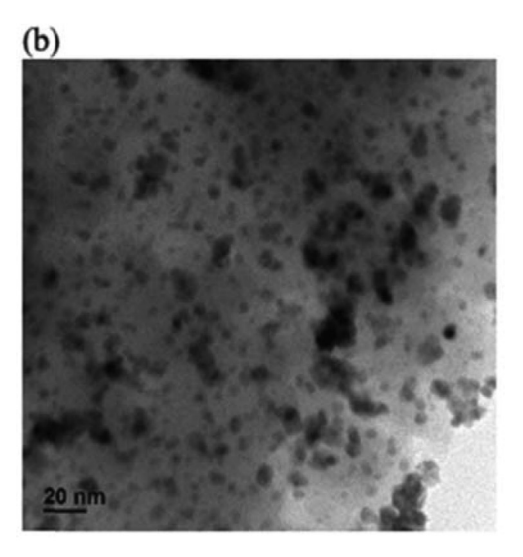
TEM was performed to obtain the size and distribution of Pd particles supported on SOMS, SOMS-UD and SOMS-PDD samples. The TEM images in Fig. 3, show that Pd was better dispersed on SOMS-UD than other supports. The corresponding particle size distributions (PSDs), shown in Fig. 4, display a narrower distribution of Pd particles on SOMS\_UD than other supports. The mean particle sizes of Pd supported on SOMS-UD, SOMS-PDD and SOMS were 5.6, 8.6 and 10.5 nm, respectively. The trend observed with the average size of Pd particles is consistent with that observed with the pore sizes of their supports: SOMS-UD < SOMS-PDD < SOMS (discussed in the previous section). It should be noted that all three supports were impregnated with Pd using identical synthesis procedure which ensures that the Pd particle size is primarily dictated by properties of the support. As shown in Fig. 3, the TEM images, though collected with same resolution, show particles with different contrasts. The darker particles appear closer to the pore mouth whereas the ones with low contrast, could be located deeper in the pores. This difference in contrasts is more apparent in the images of Pd/SOMS and Pd/SOMS-PDD than Pd/SOMS-UD. It can be said that more particles are situated closer to the pore mouth in case of Pd/SOMS-PDD than other samples. This aspect is further discussed in the sections that follow.

It can be noticed that particle size of Pd obtained from TEM is higher than the pore size for all catalysts reported in the previous section. The occurrence of larger particles inside smaller pores can be explained by considering the swellable nature of these supports. During catalyst synthesis, ethanol is used as the solvent which causes swelling and hence, expansion of pore-size. Consequently, size of the Pd particles formed inside the swollen pores will be larger than that if the pores had not swollen. This explains why Pd particle size from TEM analysis appears to be higher than the pore size obtained by N2 physisorption because the latter belongs to non-swollen support. A similar phenomenon was observed in our earlier study wherein swellability of SOMS allowed the encapsulation of externally synthesized CoMn oxide particles as large as  $\sim$  13 nm, inside its pores [15]. In summary, the sequence of derivatization affects the textural properties and swellability of the support, thereby influencing the particle size of Pd.

#### 3.4. Inductively coupled plasma - mass spectrometry (ICP-MS):

HCl, an unavoidable byproduct of HDC of TCE, is known to cause leaching of supported Pd particles [23]. The results shown in Fig. 5 convey that all catalysts yielded similar Pd leaching by HCl in presence of ethanol; however, in presence of TCE the leaching resistance was in the order: Pd/SOMS > Pd/SOMS-PDD > Pd/SOMS-UD (same as the order of their hydrophobicity per Section 3.2). This suggests that the difference in polarities of TCE and ethanol could





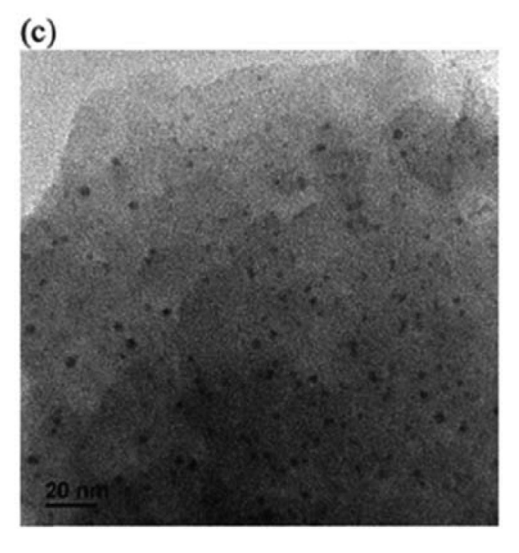


**Fig. 3.** TEM images of 1.25 %Pd supported on structurally altered SOMS: a) Pd/SOMS; b) Pd/SOMS-PDD; c) Pd/SOMS-UD.

also have played an important role during leaching. Ethanol being polar, can carry water and dissolved HCl inside the pores of all three catalysts. In contrast, TCE being non-polar, it is more selectively partitioned inside these catalysts such that majority of water and HCl (both polar species) are obstructed outside the pores. The

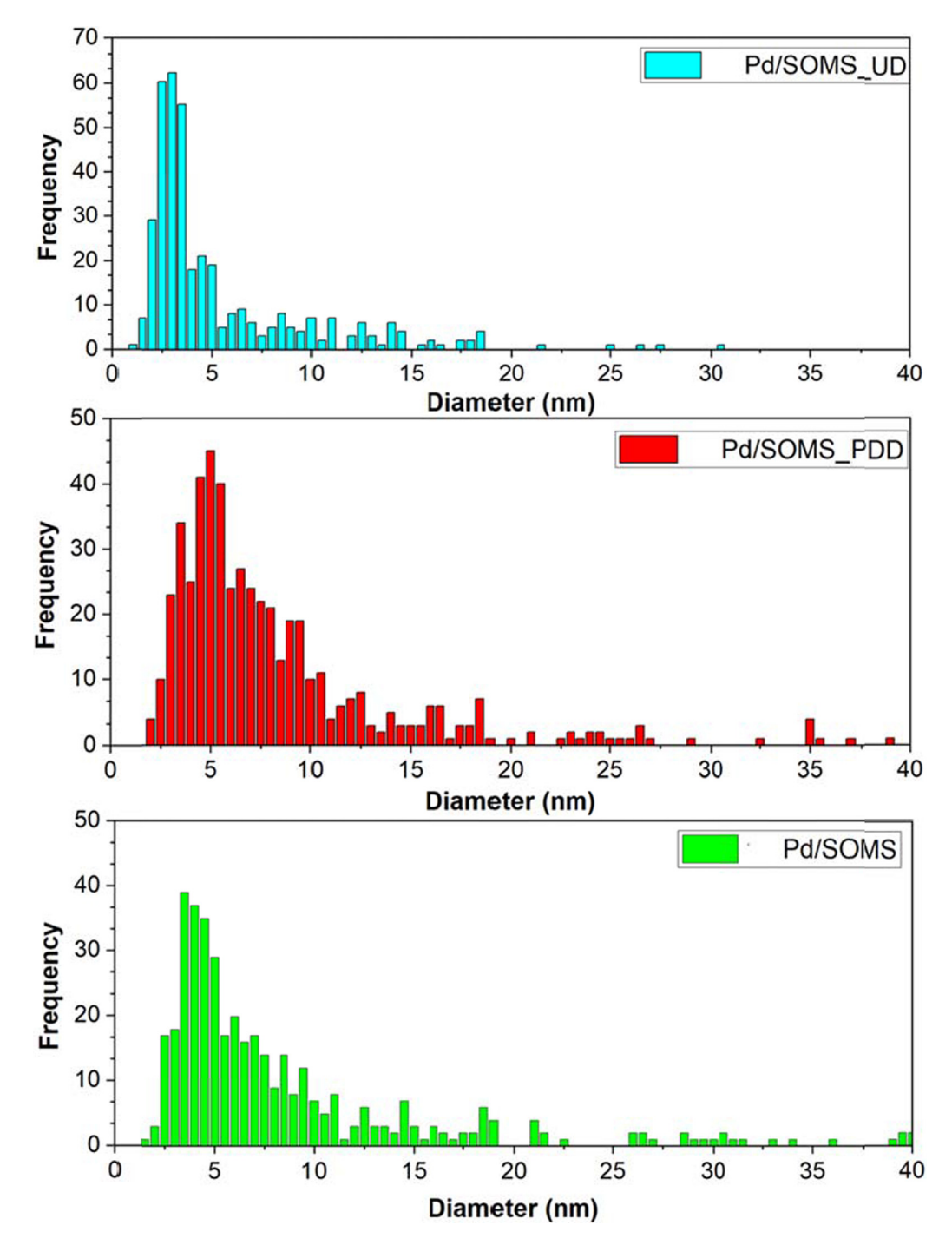


Fig. 4. Particle size distribution obtained from analysis of TEM images of Pd supported on structurally altered SOMS.

catalyst's affinity to TCE is directly proportional to its degree of hydrophobicity [19,27,81]. Therefore, with SOMS being the most hydrophobic material, it is conceivable that it should have the highest affinity to TCE. Thus, Pd can be shielded to a greater extent on SOMS than other supports.

Moreover, these experiments suggest that TCE (the main reactant), by virtue of its non-polar nature, can act as a protective agent from HCl. It can be argued that during the reaction, TCE concentration in the pores can decrease and its protection effect against external HCl molecules may decline. In this case, the swellability of these catalysts is expected to play an active role leading to closure of the pores with decreasing organic content. Recently, using

near ambient pressure X-ray photoelectron spectroscopy (NAP-XPS), we have demonstrated that the extent of swelling is directly proportional to the concentration of organics absorbed in SOMS [28]. Therefore, when the concentration of TCE depletes as reaction progresses, the swellable pores of SOMS can close, thereby protecting the Pd particles inside. Moreover, Edmiston and co-workers have reported that swelling is an instantaneous phenomenon, which implies that as soon as TCE concentration decreases, the pores of SOMS can close preventing the inward diffusion of HCl. If swelling was a slow process, the pores would have closed slowly after depletion of TCE giving HCl molecules enough time to diffuse in and cause more leaching. Support swellability decreases in the

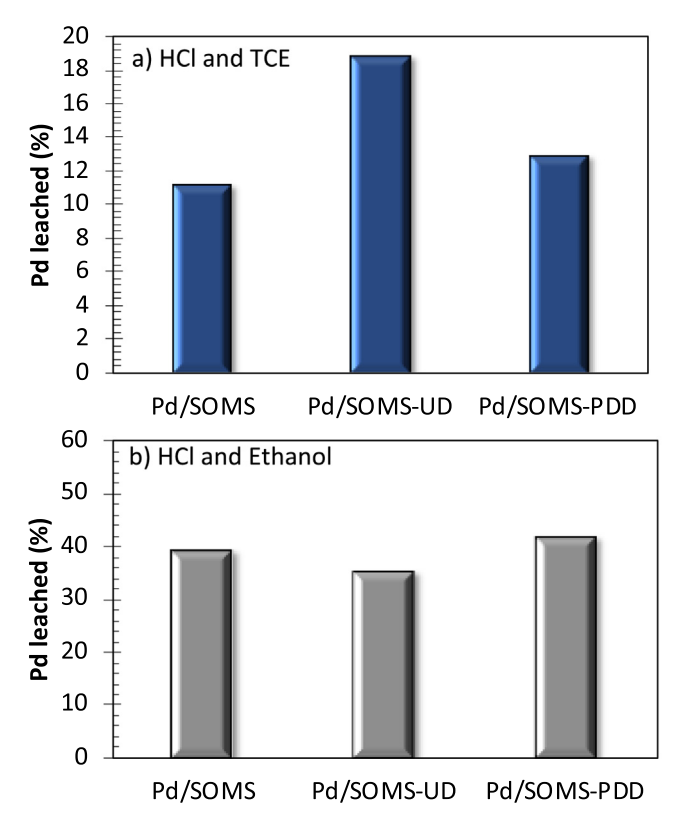


Fig. 5. Pd leaching caused due to HCl treatment in presence of TCE and ethanol using ICP-MS.

order: SOMS > SOMS-PDD > SOMS-UD (refer Section 3.1) suggesting that use of SOMS is more advantageous for preventing entry of HCl inside the pores than the other supports. Also, as seen in Section 3.3, the smaller and well-dispersed Pd particles in Pd/SOMS-UD could mean that majority of them are adhered to the support surface more strongly than in case of Pd/SOMS-PDD and Pd/SOMS (which have higher Pd size) [82]. However, leaching being worse in case of Pd/SOMS-UD under non-polar environment (i.e., in presence of TCE) the polarity of solution seems to be a more decisive factor than the particle size of Pd in determining the extent of leaching. This is also consistent with the fact that in presence of ethanol (a more polar solvent), the leaching is similar in all three cases irrespective of the difference in their particle sizes. This suggests that SOMS, owing to a combination of its high hydrophobicity and swellability, can possess high resistance to Pd leaching.

# 3.5. CO-pulsing during mass spectrometry

CO pulsing was used to reveal information regarding the total accessible sites on the catalyst surface [23]. Our previous studies have shown that SOMS has a closed pore-structure which restricts the entrance of CO inside the pores; however, when treated thermally, its pores open up allowing CO access to the internal surface where majority of the active sites are situated [15,21,26]. Adsorption profiles belonging to Pd/SOMS are published elsewhere and no CO consumption was observed as mentioned above [26]. The results shown in Fig. 6a convey that CO consumption was observed on pristine Pd/SOMS-UD and Pd/SOMS-PDD. It should be noted that CO consumption on these samples does not necessarily indicate that all Pd sites are accessible. Because of the swellability of these catalysts, a fraction of Pd sites might dwell inside closed

pores where CO cannot enter. Furthermore, CO consumption was higher on Pd/SOMS-UD than Pd/SOMS-PDD, indicating that more Pd sites are accessible in case of the former catalyst. These results complement the TEM analysis (Section 3.3), where Pd/SOMS-UD was found to have better dispersion of Pd than Pd/SOMS-PDD.

Fig. 6b shows CO chemisorption performed on HCl-treated catalysts. A significant drop in CO consumption for both the samples was observed, indicating that most of the accessible Pd sites were leached. As mentioned earlier, corrosive action of HCl results in leaching of supported Pd particles [23,50]. Moreover, CO adsorption was higher on HCl-soaked Pd/SOMS-PDD than Pd/SOMS-UD suggesting that more leaching of Pd sites occurred on the latter sample which is consistent with the ICP-MS results mentioned previously. Thus, CO pulsing performed in gas phase can probe the exterior surface and reveal the extent of Pd leached.

# 3.6. X-ray photoelectron spectroscopy (XPS)

XPS was used to investigate the changes occurring on the surface of Pd/SOMS, Pd/SOMS-UD and Pd/SOMS-PDD after soaking them in HCl. The Pd 3d region of spectra shown in Fig. 7a, revealed that pristine Pd/SOMS-PDD and Pd/SOMS-UD exhibited higher surface Pd signals than Pd/SOMS. This is consistent with the fact that negligible CO chemisorption was observed on Pd/SOMS (Section 3.5). Thus, XPS data also suggests that Pd is located well inside the closed pores of SOMS. Similarly, our previous study reported that etching the surface of Pd/SOMS with Ar- ions revealed Pd signals with increasing intensity implying that the Pd particles situated deeper inside the pores were exposed after etching [26]. Fig. 7a shows that Pd species on Pd/SOMS-PDD and Pd/SOMS-UD could be situated closer to the surface than on Pd/SOMS. It follows that, during XPS, kinetic energy (K.E.) of the photoelectrons (of Pd) evolving from Pd/SOMS, is attenuated after their collision with the closed matrix of SOMS. The matrix of Pd/SOMS-UD and Pd/SOMS-PDD being more open, the photoelectrons ejected from these catalysts may face less hindrance by the support matrix and hence, can reach the XPS detector with higher K.E revealing the presence of surface Pd.

Furthermore, the Pd surface atomic concentration (refer Table 2) is higher on pristine Pd/SOMS-PDD than Pd/SOMS-UD which seems to be contradictory to the CO chemisorption results. This can be reconciled by considering the difference in their Pd particle size distribution. As mentioned in Section 3.3, Pd particles are more uniformly distributed on Pd/SOMS-UD than Pd/SOMS-PDD. Therefore, for Pd/SOMS-PDD, non-uniform distribution of Pd particles could mean that some particles are situated close to the pore mouth resulting in high intensity of surface Pd spectra.

When these catalysts were soaked in HCl, Pd signals dropped drastically indicating the occurrence of Pd leaching (Fig. 7b). As a result of leaching, the decrease in the atomic concentration of surface Pd species was in the order: Pd/SOMS-UD > Pd/SOMS-PDD > Pd/SOMS (refer Table 2), same as their relative hydrophobicities. Although Pd particles seem to be concentrated near the pore mouth of Pd/SOMS-PDD than Pd/SOMS-UD, the latter suffered from more Pd loss, post-HCl-soaking. This shows that low hydrophobicity of Pd/SOMS-UD allowed HCl to penetrate deeper in its pores resulting in significant decrease in the overall surface Pd signals. This is also consistent with CO chemisorption results wherein CO consumption decreased significantly on Pd/SOMS-UD.

The intensity of Cl 2p signals (Fig. S2) of these samples can be correlated to the intensity of their Pd 3d signals after HCl soaking suggesting that chloride is more likely to be bound to the Pd surface than the support. Thus, HCl soaking primarily led to leaching of Pd particles, but, it also caused chlorination of the remaining

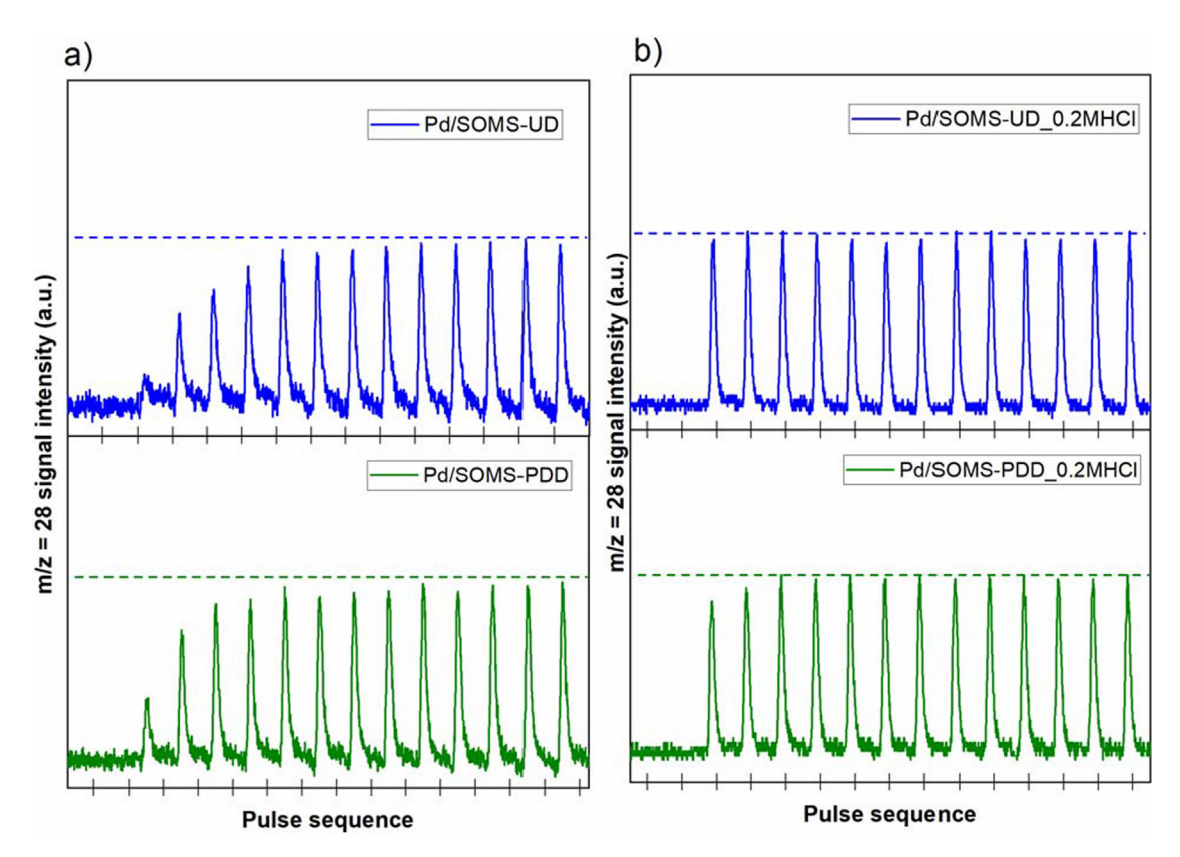


Fig. 6. CO chemisorption on pristine and HCl treated Pd/SOMS-UD and Pd/SOMS-PDD using mass spectrometry.

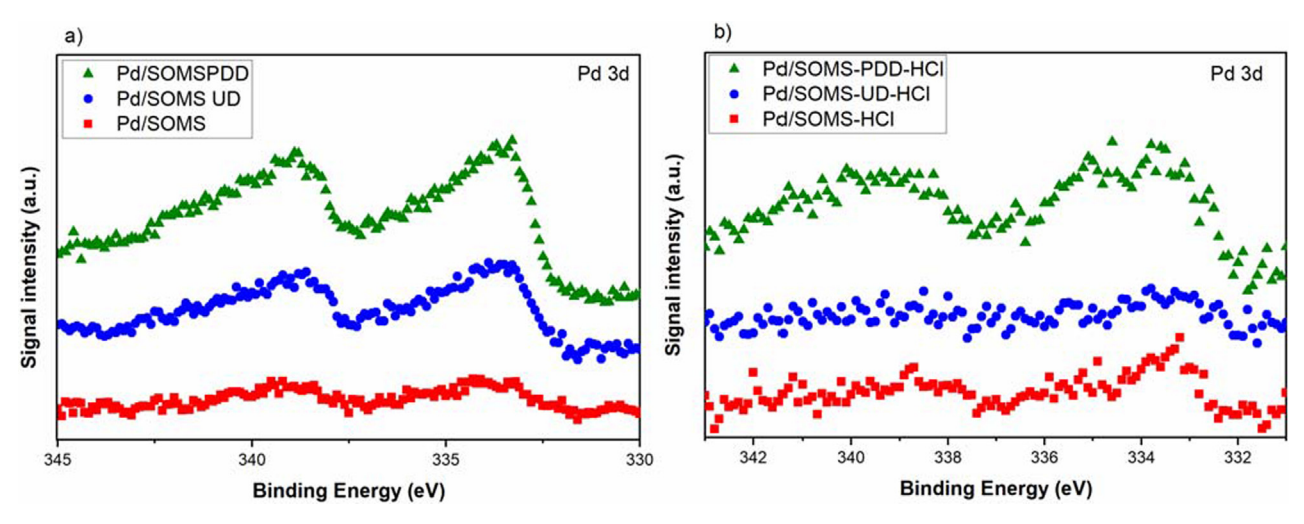


Fig. 7. XPS spectra showing Pd 3d region of pristine and HCl soaked Pd/SOMS, Pd/SOMS-PDD and Pd/SOMS-UD.

**Table 2**Surface atomic concentration of Pd on pristine and HCl treated catalysts.

Sample	Pristine (%)	Treated with HCl (%)	Decrease after HCl treatment (%)
Pd/SOMS	0.16	0.11	31
Pd/SOMS-UD	0.38	0.05	87
Pd/SOMS-PDD	0.68	0.24	65

Pd particles. Overall, derivatization of the support can help repel majority of HCl dissolved in water by imparting hydrophobicity to the material, thereby preventing Pd leaching.

# 3.7. Extended X-ray absorption fine edge structure (EXAFS)

Changes occurring in the atomic environment of Pd in Pd/SOMS, Pd/SOMS-UD and Pd/SOMS-PDD after soaking them in HCl, were investigated using EXAFS. Fourier transform (FT) magnitudes of  $k^2$  weighted Chi(k) (uncorrected for amplitude and phase shifts) for catalysts soaked in HCl solutions containing ethanol and TCE are shown in Fig. 8 and Fig. 9 respectively. The corresponding fitting results provided in Table S1, were within the error range of EXAFS analysis [83]. These results show that, the co-ordination numbers (CNs) of Pd-Pd scattering for all the catalysts were in the order: Pd/SOMS-UD < Pd/SOMS-PDD < Pd/SOMS which is

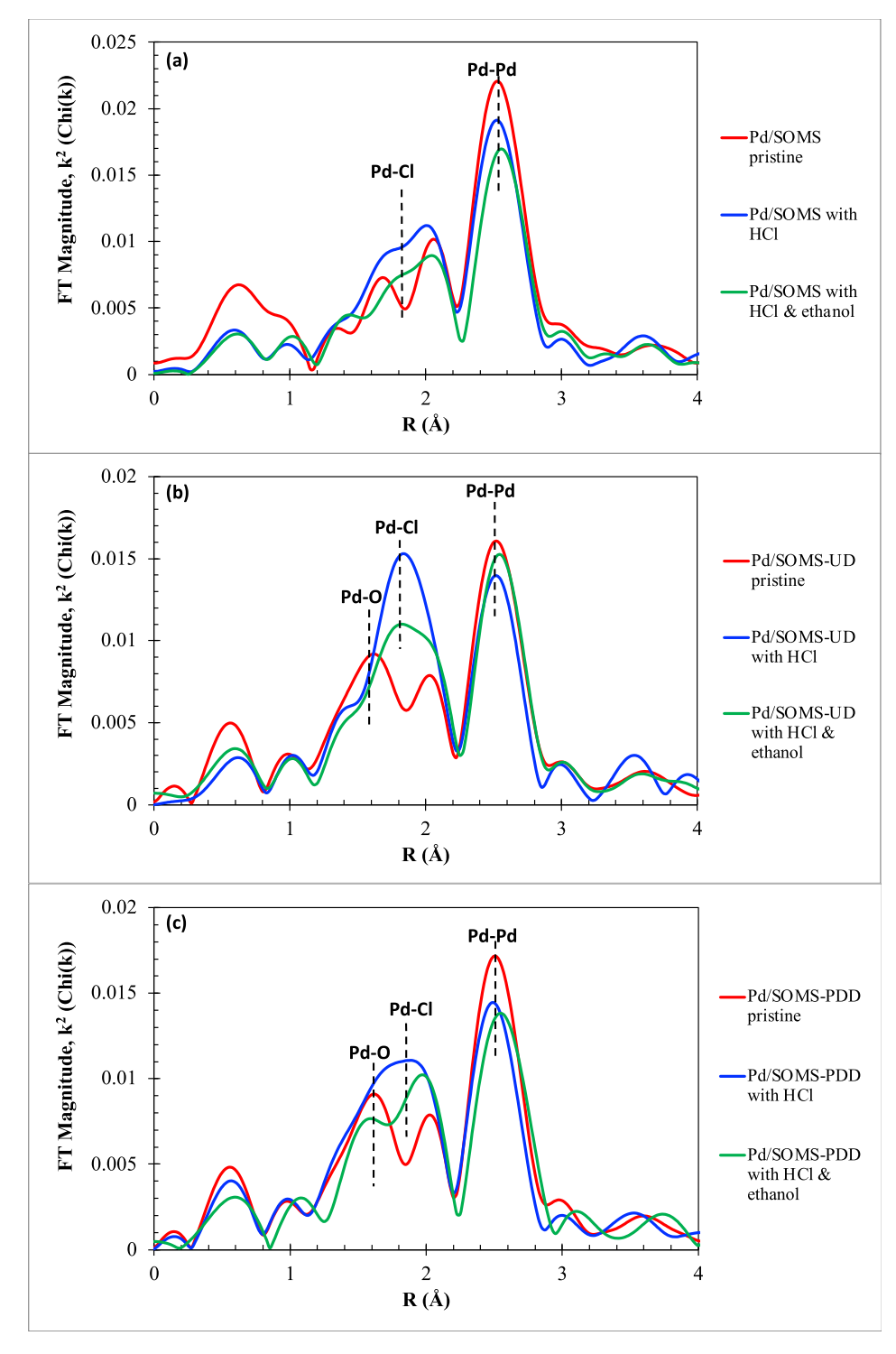


Fig. 8. Pd K-edge spectra showing changes in the atomic environment of 1.25 %Pd supported on SOMS, SOMS-UD and SOMS-PDD after soaking in HCl solutions with and without ethanol.

consistent with the trend shown by TEM (Section 3.3.), as the CN of reduced transition metal nanoparticles is generally found to be directly proportional to its average particle size [83].

From the FT magnitudes, Pd-O and Pd-Pd interactions can be observed in case of pristine Pd/SOMS-UD and Pd/SOMS-PDD whereas only Pd-Pd interactions are seen in case of pristine Pd/SOMS (for convenience, a comparison of the pristine samples alone is shown in Fig.S3). Also, the threshold energy value of Pd/SOMS matched more closely to that of Pd<sup>0</sup> (24,350 eV) whereas for Pd/

SOMS-UD and Pd/SOMS-PDD they shifted towards higher values (indicating the presence of oxidized species). The Pd-O species observed on Pd/SOMS-UD and Pd/SOMS-PDD could be due to oxidation of reduced Pd upon exposure to atmosphere. Such an oxidation was not observed on Pd/SOMS because majority of the Pd particles are situated deep inside the closed pores of SOMS (shown by XPS and CO pulsing above). In fact, these Pd particles were not accessible to gas phase CO molecules (Section 3.5) which also implies that they may not be accessible to gas phase O<sub>2</sub> molecules

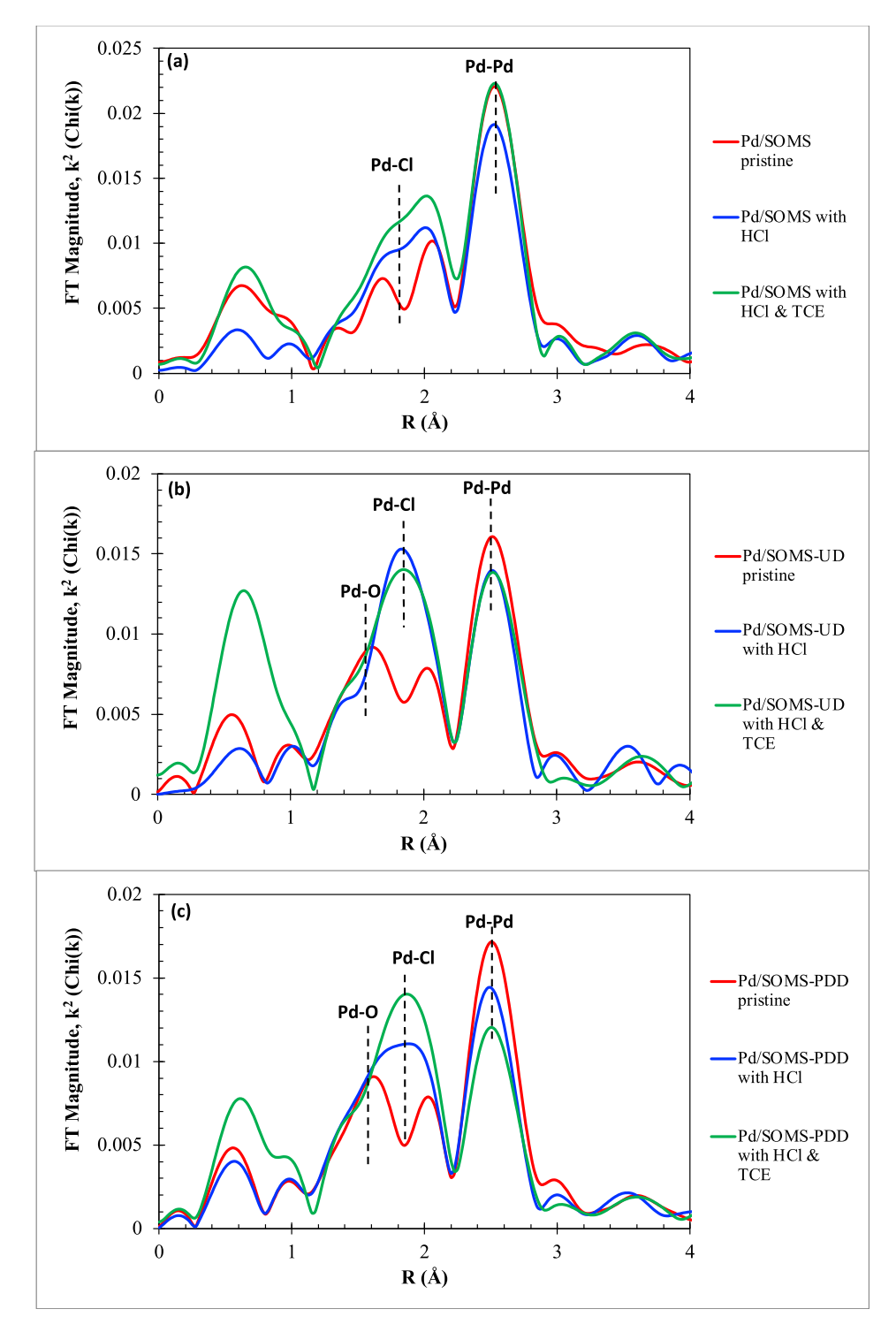


Fig. 9. Pd K-edge spectra showing changes in the atomic environment of 1.25 %Pd supported on SOMS, SOMS-UD and SOMS-PDD after soaking in HCl solutions with and without TCE.

in air. This protection offered by the flexible SOMS matrix to embedded metal particles makes its application as a catalytic support material desirable from a stability point of view.

When these samples were soaked in an aqueous solution of HCl, new Pd-Cl bonds were observed (accompanied by a decrease in Pd-Pd), accompanied by a shift in the threshold energy towards higher values, indicative of an increase in the Pd oxidation state [84]. The FT magnitudes of the chloride containing samples shown in Fig. 8 agree with those reported for a chlorinated  $Pd/Al_2O_3$  catalyst by

Newton et al [85]. Moreover, maximum Pd-Cl formation was observed on Pd/SOMS-UD, showing that the least hydrophobic catalyst (Pd/SOMS-UD) was most prone to chlorination by HCl.

When HCl soaking was performed in presence of TCE, Pd-Cl CNs of Pd/SOMS-UD and Pd/SOMS-PDD were similar, whereas they were slightly higher for Pd/SOMS (Fig. 9). This behavior can be explained by considering that, during soaking, selective sorption of TCE inside the pores of Pd/SOMS may restrict the entry of water and HCl however, the cleavage of C-Cl bonds of TCE on Pd may

itself contribute to Pd-Cl formation in Pd/SOMS [28,86,87]. Therefore, in this study, the slightly higher chlorination on Pd/SOMS compared to the other two catalysts could be due to high TCE sorption rather than HCl sorption. In case of Pd/SOMS-UD, the Pd-Cl interactions formed after HCl-soaking, with and without TCE, were almost similar. As mentioned above, sorption of TCE in the pores can lower the sorption of water and HCl around the active sites. Therefore, though Pd chlorination caused by HCl may decrease, it can be compensated by chlorination caused by TCE itself (thereby showing a no net change in the Pd-Cl CN).

Addition of ethanol during HCl soaking decreased the extent of Pd chlorination for all samples (Fig. 9) despite swelling caused by the presence of ethanol, which would be expected to cause a higher degree of chlorination. In our previous study, in-situ X-ray absorption near edge structure (XANES) spectroscopy showed that ethanol dissolved in water can reduce Pd<sup>2+</sup> species under atmospheric conditions [27]. Owing to this reducing nature of ethanol, chlorination of Pd by HCl was suppressed for all three catalysts, even though swelling due to ethanol may have exposed all Pd sites to HCl. Moreover, the Pd-O species originally present in the sample were also reduced, further increasing the Pd-Pd interactions [88]. Lastly, Pd chlorination was found to be the highest on the least hydrophobic catalyst i.e., Pd/SOMS-UD, even in presence of ethanol, underscoring the importance of catalyst hydrophobicity.

## 3.8. Catalytic activity experiments

# 3.8.1. Activity of pristine catalysts

Fig. 10 shows TCE conversion obtained during HDC reactions performed in the presence and absence of ethanol. In absence of ethanol, the catalytic activity is in the order: Pd/SOMS-UD > Pd/SOMS-PDD > Pd/SOMS, which can be inversely related to the mean particle size of Pd on these samples. As shown by EXAFS analysis, a small fraction of Pd/SOMS-UD and Pd/SOMS-PDD was found to be oxidized; however, that small fraction might undergo rapid reduction by H<sub>2</sub> at the beginning of the reaction. A proof of this phenomenon was reported in our earlier study where in-situ X-ray absorption near edge structure (XANES) revealed that H<sub>2</sub> dissolved in water could reduce oxidized Pd species supported on SOMS even under ambient conditions [27]. In the batch experiments performed in this study, the operating H<sub>2</sub> pressure is much higher than ambient conditions (i.e., 50 bar), that could result in accelerated reduction of residual oxidized Pd species in Pd/SOMS-UD and Pd/SOMS-PDD

A plateau was observed in the conversion ( $X_{TCE}$ ) vs time plot of Pd/SOMS at 240 min (Fig. 10c) because HCl produced during HDC gets accumulated inside the pores while the  $H_2$  concentration is depleted, resulting in plateau or catalyst deactivation (Fig. 10c) [28]. This catalyst deactivation can be avoided by maintaining high  $[H_2]/[HCl]$  ratio which discourages the adsorption of HCl on the Pd sites [28]. The plateau is much less prominent for Pd/SOMS-UD and Pd/SOMS-PDD. Pd/SOMS-UD being hydrophilic, allows water molecules to reach inside the pores and act as a medium for HCl removal while maintaining high  $H_2$  supply. For Pd/SOMS-PDD, XPS and CO chemisorption results suggested that a fraction of Pd particles might be situated closer to the pore mouths where they are easily accessible to  $H_2$  even under less swollen conditions (causing less HCl accumulation).

Addition of ethanol proved to be beneficial for all three catalysts resulting in higher  $X_{TCE}$  at the end of 240 min for all catalysts (Fig. 10). Pd/SOMS being the most swellable support, effect of ethanol was most prominent on its performance. Pd/SOMS-UD and Pd/SOMS-PDD both being partially swellable, addition of ethanol benefited their catalytic performances as well. Had the pores of these catalysts been completely rigid, the enhancement in their performance by ethanol addition may not have been observed like Pd/

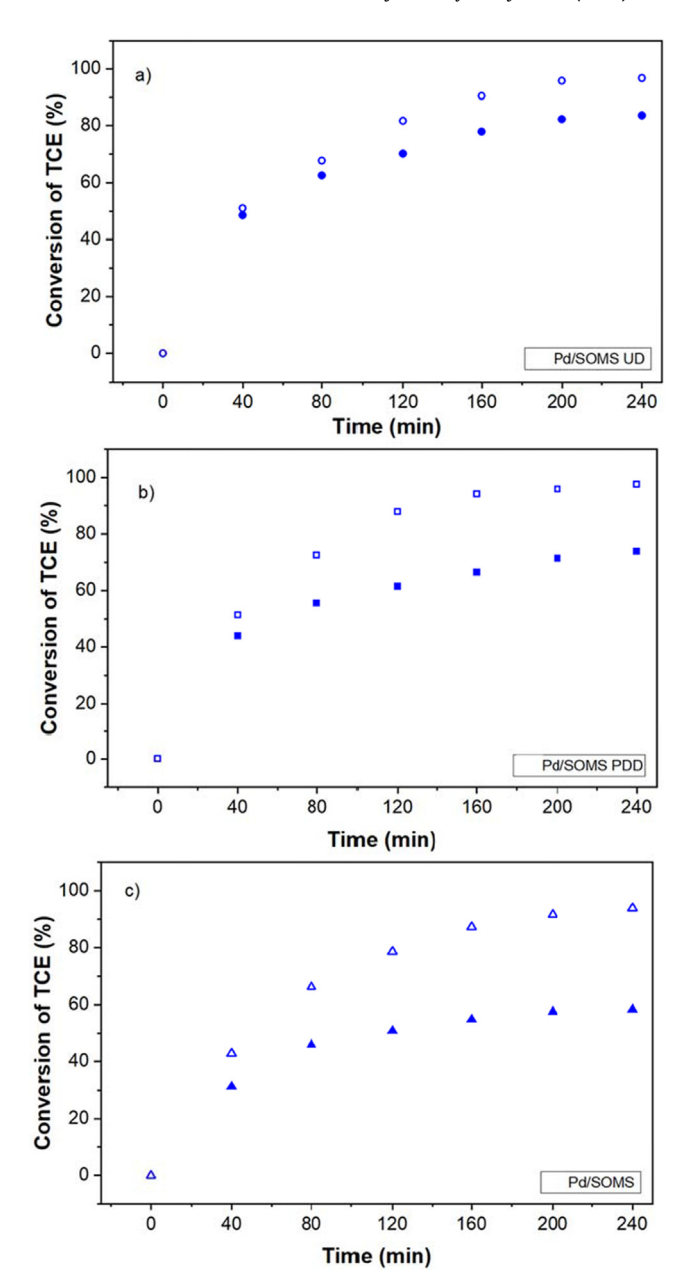


**Fig. 10.** Catalytic performance of pristine (a) Pd/SOMS-UD, (b) Pd/SOMS-PDD and (c) Pd/SOMS. Hollow symbols: In the presence of 10% ethanol and Solid symbols: In absence ethanol; 5 mg catalyst, 1.25 %Pd, 30 °C and 50 bar of pure  $\rm H_2$ .

Al<sub>2</sub>O<sub>3</sub> (non-swellable catalyst), which showed no change in activity after the addition of ethanol [26]. Lastly, in our recent study focusing on the mechanism of HDC of TCE, it was shown that ethanol does not alter the reaction pathway using Pd [28].

# 3.8.2. Activity of HCl-treated samples

When these catalysts were soaked in aqueous solution of HCl prior to their addition to the reactor, their performance was lower (Fig. 11) compared to their pristine counterparts. The decrease in TCE conversion was in the order Pd/SOMS > Pd/SOMS-PDD > Pd/S OMS-UD (same order as their resistance to leaching by HCl). The behavior of Pd/SOMS-UD is similar to Pd/Al $_2$ O $_3$  which also showed high pristine activity initially but deactivated more than Pd/SOMS after HCl treatment (both ex-situ and in-situ) [2328]. Furthermore, as shown in Fig. 11, the activity trend in presence of ethanol for catalysts treated ex-situ with HCl was: Pd/SOMS > Pd/SOMS-PD

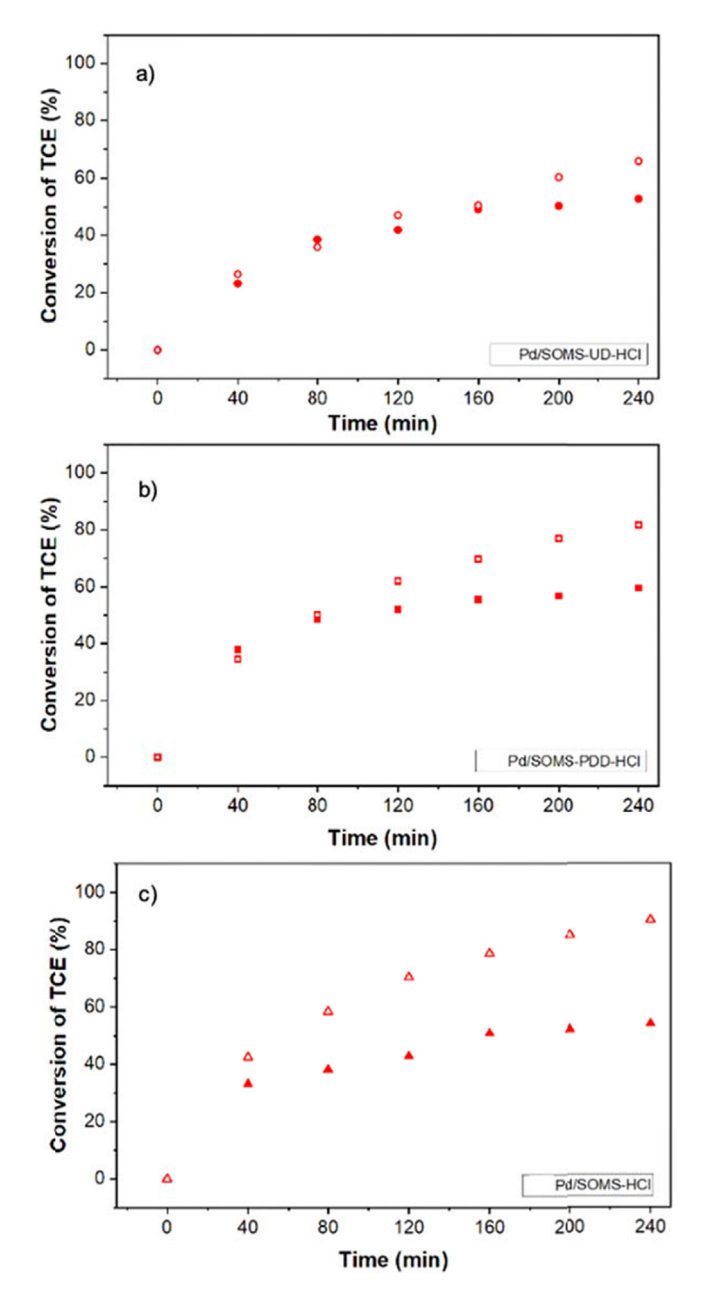


**Fig. 11.** Catalytic performance HCl soaked (a) Pd/SOMS-UD, (b) Pd/SOMS-PDD and (c) Pd/SOMS. Hollow symbols: In the presence of 10% ethanol and Solid symbols: In absence ethanol; 5 mg catalyst, 1.25 %Pd, 30 °C and 50 bar of pure  $\rm H_2$ .

D > Pd/SOMS-UD. Pd/SOMS-UD having high hydrophilicity and low swellability, was observed to have the highest drop in activity compared to its pristine counterpart. Pd/SOMS-PDD having intermediate swellability and hydrophobicity, displayed an intermediate drop in activity. The activity of ex-situ HCl-treated Pd/SOMS (highest hydrophobicity and swellability) was slightly lower than its pristine counterpart revealing that majority of its Pd sites were protected. The swellable nature of SOMS helps in creating a physical protection for the Pd particles from HCl molecules during exsitu soaking in aqueous solution.

Lastly, in our earlier studies, it was found that addition of ethanol led to first order behavior with respect to TCE, on Pd/SOMS [28]. It should be noted that kinetic analysis cannot be performed for the reactions without ethanol, because the matrix cannot be kept swollen throughout the reaction which changes the availability of active Pd sites constantly. Therefore, for both pristine and

HCl-treated samples, linear plots of conversion vs time in presence of ethanol were obtained (Fig. 12). The pseudo first order rate constants were obtained from the slopes of the linear fits. Upon comparing the pristine and HCl-treated catalysts, decrease in the rate constant was observed after HCl treatment by 66%, 56% and 17% for Pd/SOMS-UD, Pd/SOMS-PDD and Pd/SOMS respectively. This trend is consistent with that corresponding to the deactivation of Pd sites from each sample as shown by XPS and EXAFS analysis. Thus, Pd/SOMS-UD and Pd/SOMS-PDD performed better than Pd/SOMS in their pristine and only marginally better in their swollen form, however, they lacked the deactivation resistance displayed by Pd/SOMS.

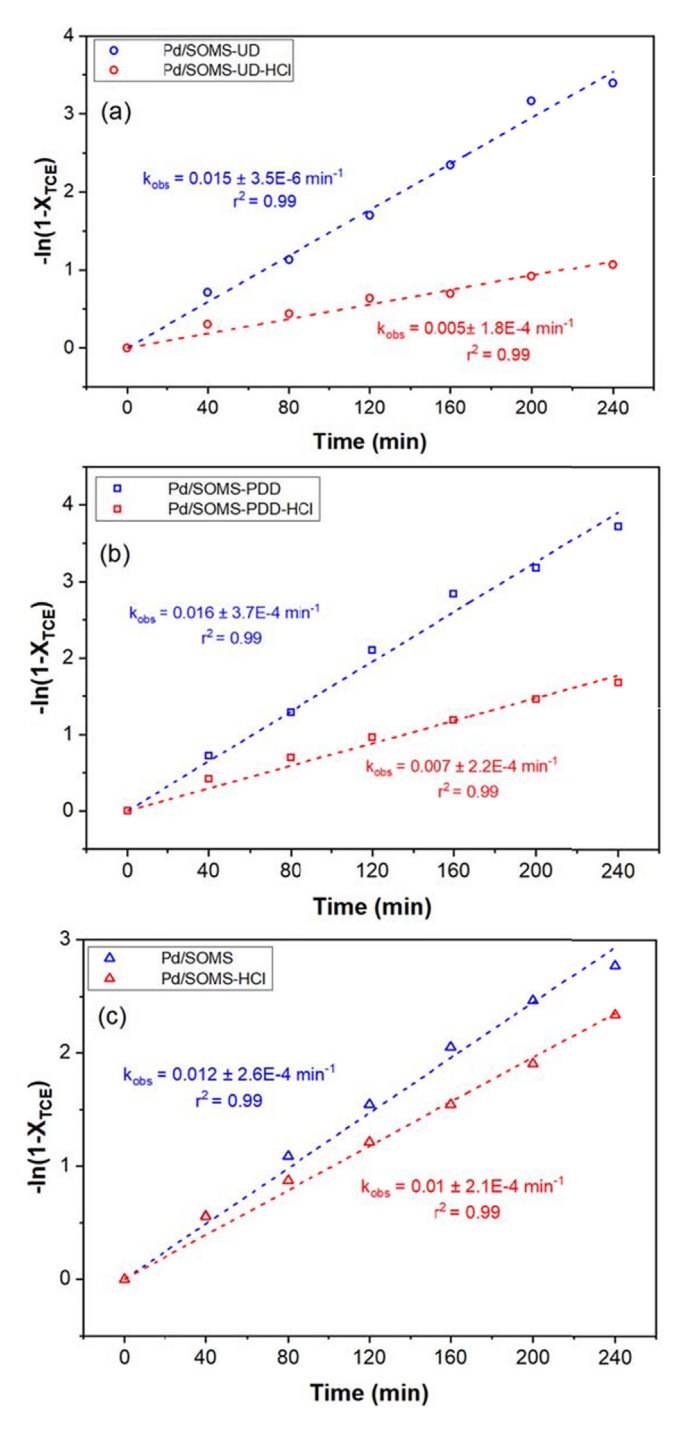


Fig. 12. Linearized plots of activity data in presence of ethanol with and without HCl treatment; 5 mg catalyst, 1.25% Pd, 30  $^{\circ}$ C and 50 bar of pure  $H_2$ .

#### 4. Conclusions

Derivatization performed during synthesis of SOMS determines its extent of hydrophobicity and swellability. Derivatized samples were more hydrophobic than the underivatized (SOMD-UD) one; however, when derivatization was performed prior to drying (SOMS), the material obtained was more swellable than the one where derivatization was performed post-drying (SOMS-PDD).

When Pd was deposited on these supports, the resulting Pd particle size was found to follow the same trend as the swellability of these catalysts: Pd/SOMS > Pd/SOMS-PDD > Pd/SOMS-UD. Pd particle distribution was also dictated by the support: uniform distribution on SOMS-UD, deep inside the pores on SOMS and, near pore mouth on SOMS-PDD.

Pristine catalytic activity tests showed that the hydrophilic and least swellable catalyst (Pd/SOMS-UD) was most active due to its smaller Pd particle size and open pore structure. However, after HCl treatment, Pd/SOMS-UD showed the highest loss in activity. Pd/SOMS, on the other hand, was found to be the most active catalyst post HCl-treatment. The closed pore structure and hydrophobicity of SOMS allows the Pd particles to be shielded from HCl molecules dissolved in water. Addition of ethanol during the activity testing led to swelling of these catalysts and first order kinetics. On comparing the first order rate constants of pristine and HCl treated catalysts, the highest decrease in rate constant was found for Pd/SOMS-UD (hydrophilic and least swellable) whereas the least drop was found on Pd/SOMS (hydrophobic and most swellable). This led to the conclusion that, not only hydrophobicity but, swellability is also a key factor in imparting deactivation resistance from HCl. These properties make SOMS a more attractive choice as a catalyst support for HDC of TCE.

# **Declaration of Competing Interest**

The authors declare that they have no known competing financial interests or personal relationships that could have appeared to influence the work reported in this paper.

# Acknowledgements

This work was financially supported by the National Science Foundation through the Grant CBET- 1436729. J.T.M. was supported as part of the National Science Foundation Energy Research Center for Innovative and Strategic Transformation of Alkane Resources (CISTAR) under the Cooperative Agreement No. EEC-1647722. EXAFS data was collected at the Materials Research Collaborative Access Team's (MRCAT) sector 10- ID-B at Argonne National Laboratory. MRCAT operations are supported by the Department of Energy and the MRCAT member institutions. This research used resources of the Advanced Photon Source, a U.S. Department of Energy (DOE) Office of Science User Facility operated for the DOE Office of Science by Argonne National Laboratory under Contract No. DE-ACO2-06CH11357. The authors would like to thank Dr. Yehia Khalifa and Dr. Anthony Lutton for assistance with XPS and ICP-MS data collection.

# Appendix A. Supplementary material

Supplementary data to this article can be found online at https://doi.org/10.1016/j.jcat.2022.04.031.

#### References

- [1] K.J. Shea, D.A. Loy, Bridged polysilsesquioxanes. Molecular-engineered hybrid organic—inorganic materials, Chem. Mater. 13 (2001) 3306–3319.
- [2] K. Shea, D.A. Loy, O. Webster, Arylsilsesquioxane gels and related materials. New hybrids of organic and inorganic networks, J. Am. Chem. Soc. 114 (1992) 6700–6710.
- [3] D.A. Loy, K.J. Shea, Bridged polysilsesquioxanes. Highly porous hybrid organic-inorganic materials, Chem. Rev. 95 (1995) 1431–1442.
- [4] G. Cerveau, R.J. Corriu, E. Framery, S. Ghosh, H.P. Mutin, Hybrid materials and silica: drastic control of surfaces and porosity of xerogels via ageing temperature, and influence of drying step on polycondensation at silicon, J. Mater. Chem. 12 (2002) 3021–3026.
- [5] C.M. Burkett, L.A. Underwood, R.S. Volzer, J.A. Baughman, P.L. Edmiston, Organic-inorganic hybrid materials that rapidly swell in non-polar liquids: nanoscale morphology and swelling mechanism, Chem. Mater. 20 (2008) 1312–1321.
- [6] C.M. Burkett, P.L. Edmiston, Highly swellable sol–gels prepared by chemical modification of silanol groups prior to drying, J. Non-Cryst. Solids 351 (2005) 3174–3178.
- [7] J.D. Sunseri, W.T. Cooper, J.G. Dorsey, Reducing residual silanol interactions in reversed-phase liquid chromatography: Thermal treatment of silica before derivatization, J. Chromatogr. A 1011 (2003) 23–29.
- [8] V. Gun'Ko, M. Vedamuthu, G. Henderson, J. Blitz, Mechanism and kinetics of hexamethyldisilazane reaction with a fumed silica surface, J. Colloid Interface Sci. 228 (2000) 157–170.
- [9] J.H. Song, M.J. Sailor, Chemical modification of crystalline porous silicon surfaces, Comments Inorg. Chem. 21 (1999) 69–84.
- [10] H. Yang, G. Zhang, X. Hong, Y. Zhu, Silylation of mesoporous silica MCM-41 with the mixture of Cl (CH2) 3SiCl3 and CH3SiCl3: combination of adjustable grafting density and improved hydrothermal stability, Microporous Mesoporous Mater. 68 (2004) 119–125.
- [11] A. Berthod, Silica: backbone material of liquid chromatographic column packings, J. Chromatogr. A 549 (1991) 1–28.
- [12] M. Ojeda, F.J. Pérez-Alonso, P. Terreros, S. Rojas, T. Herranz, M. López Granados, J.L.G. Fierro, Silylation of a Co/SiO<sub>2</sub> catalyst. Characterization and exploitation of the CO hydrogenation reaction, Langmuir 22 (2006) 3131–3137.
- [13] N.A. Fellenz, J.F. Bengoa, M.V. Cagnoli, S.G. Marchetti, Changes in the surface hydrophobicity degree of a MCM-41 used as iron support: a pathway to improve the activity and the olefins production in the Fischer-Tropsch synthesis, J. Porous Mater. 24 (2017) 1025–1036.
- [14] R. Xie, D. Li, B. Hou, J. Wang, L. Jia, Y. Sun, Silylated Co<sub>3</sub>O<sub>4</sub>-m-SiO<sub>2</sub> catalysts for Fischer-Tropsch synthesis, Catal. Commun. 12 (2011) 589–592.
- [15] D. Basu, S. Ailawar, G. Celik, P. Edmiston, U.S. Ozkan, Effect of high temperature on swellable organically modified silica (SOMS) and its application for preferential CO oxidation in H<sub>2</sub> rich environment, ChemCatChem 12 (2020) 3753–3768.
- [16] D.J. Kim, B.C. Dunn, P. Cole, G. Turpin, R.D. Ernst, R.J. Pugmire, M. Kang, J.M. Kim, E.M. Eyring, Enhancement in the reducibility of cobalt oxides on a mesoporous silica supported cobalt catalyst, Chem. Commun. (2005) 1462–1464
- [17] S. Yuanyuan, L. Kongyong, L. Jinlin, Effect of silylation of SBA-15 on its supported cobalt catalysts for Fischer-Tropsch synthesis, Chin. J. Catal. 30 (2009) 1091–1095.
- [18] P.L. Edmiston, L.J. West, A. Chin, N. Mellor, D. Barth, Adsorption of gas phase organic compounds by swellable organically modified silica, Ind. Eng. Chem. Res. 55 (2016) 12068–12079.
- [19] P.L. Edmiston, L.A. Underwood, Absorption of dissolved organic species from water using organically modified silica that swells, Sep. Purif. Technol. 66 (2009) 532–540.
- [20] E.K. Stebel, K.A. Pike, H. Nguyen, H.A. Hartmann, M.J. Klonowski, M.G. Lawrence, R.M. Collins, C.E. Hefner, P.L. Edmiston, Absorption of short-chain to long-chain perfluoroalkyl substances using swellable organically modified silica, Environ. Sci. Water Res. Technol. 5 (2019) 1854–1866.
- [21] H. Sohn, G. Celik, S. Gunduz, S.S. Majumdar, S.L. Dean, P.L. Edmiston, U.S. Ozkan, Effect of high-temperature on the swellable organically-modified silica (SOMS) and its application to gas-phase hydrodechlorination of trichloroethylene, Appl. Catal. B 209 (2017) 80–90.
- [22] H. Sohn, G. Celik, S. Gunduz, S.L. Dean, E. Painting, P.L. Edmiston, U.S. Ozkan, Hydrodechlorination of trichloroethylene over Pd supported on swellable organically-modified silica (SOMS), Appl. Catal. B 203 (2017) 641–653.
- [23] G. Celik, S.A. Ailawar, S. Gunduz, J.T. Miller, P.L. Edmiston, U.S. Ozkan, Aqueous-phase hydrodechlorination of trichloroethylene over Pd-based swellable organically-modified silica (SOMS): Catalyst deactivation due to chloride anions, Appl. Catal. B 239 (2018) 654–664.
- [24] G. Celik, S.A. Ailawar, S. Gunduz, J.T. Miller, P.L. Edmiston, U.S. Ozkan, Aqueous-phase hydrodechlorination of trichloroethylene over pd-based swellable organically modified silica: catalyst deactivation due to sulfur species, Ind. Eng. Chem. Res. 58 (2019) 4054–4064.
- [25] G. Celik, S.A. Ailawar, S. Gunduz, P.L. Edmiston, U.S. Ozkan, Formation of carbonaceous deposits on Pd-based hydrodechlorination catalysts: Vibrational spectroscopy investigations over Pd/Al2O3 and Pd/SOMS, Catal. Today 323 (2019) 129–140.

- [26] G. Celik, S.A. Ailawar, H. Sohn, Y.u. Tang, F.F. Tao, J.T. Miller, P.L. Edmiston, U.S. Ozkan, Swellable Organically-modified Silica (SOMS) as a catalyst scaffold for catalytic treatment of water contaminated with trichloroethylene, ACS Catal. 8 (8) (2018) 6796-6809.
- [27] S. Ailawar, A. Hunoor, B. Rudzinski, G. Celik, L. Burel, J.-M. Millet, J.T. Miller, P.L. Edmiston, U.S. Ozkan, On the dual role of the reactant during aqueous phase Hydrodechlorination of Trichloroethylene (HDC of TCE) using Pd supported on Swellable Organically Modified Silica (SOMS), Appl. Catal. B 291 (2021) 120060.
- [28] S. Ailawar, A. Hunoor, Y. Khalifa, J.T. Miller, P.L. Edmiston, U.S. Ozkan, Elucidating the role of ethanol in aqueous phase hydrodechlorination of trichloroethylene over Pd catalysts supported on swellable organically modified silica (SOMS), Appl. Catal. B 285 (2021) 119819.
- [29] G.V. Lowry, M. Reinhard, Hydrodehalogenation of 1- to 3-Carbon Halogenated Organic Compounds in Water Using a Palladium Catalyst and Hydrogen Gas, Environ Sci Technol 33 (11) (1999) 1905–1910.
- [30] G.V. Lowry, M. Reinhard, Pd-Catalyzed TCE Dechlorination in groundwater: solute effects, biological control, and oxidative catalyst regeneration, Environ. Sci. Technol. 34 (2000) 3217-3223.
- [31] G.V. Lowry, M. Reinhard, Pd-catalyzed TCE dechlorination in water: effect of [H<sub>2</sub>](aq) and H<sub>2</sub>-utilizing competitive solutes on the TCE dechlorination rate and product distribution, Environ. Sci. Technol. 35 (2001) 696-702.
- [32] B.P. Chaplin, M. Reinhard, W.F. Schneider, C. Schüth, J.R. Shapley, T.J. Strathmann, C.J. Werth, Critical review of Pd-based catalytic treatment of priority contaminants in water, Environ. Sci. Technol. 46 (7) (2012) 3655-
- [33] M.A. Keane, Supported transition metal catalysts for hydrodechlorination reactions, ChemCatChem 3 (5) (2011) 800-821.
- [34] F.-D. Kopinke, K. Mackenzie, R. Köhler, Catalytic hydrodechlorination of groundwater contaminants in water and in the gas phase using Pd/ $\gamma$ -Al2O3, Appl. Catal. B 44 (1) (2003) 15–24.
- [35] P.J. Squillace, C.V. Price, Urban land-use study plan for the National Water-Quality Assessment Program, US Geol. Survey; Branch Information Services [distributor] (1996).
- [36] A. Azzellino, L. Colombo, S. Lombi, V. Marchesi, A. Piana, M. Andrea, L. Alberti, Groundwater diffuse pollution in functional urban areas: The need to define anthropogenic diffuse pollution background levels, Sci. Total Environ. 656
- [37] M.J. Moran, Occurrence and implications of selected chlorinated solvents in ground water and source water in the United States and in drinking water in 12 northeast and mid-Atlantic states, 1993-2002, Sci. Investigations Rep.
- [38] A. Aschengrau, M.R. Winter, L.G. Gallagher, V.M. Vieira, L.J. Butler, M.P. Fabian, J.L. Carwile, A.K. Wesselink, S. Mahalingaiah, P.A. Janulewicz, J.M. Weinberg, T. F. Webster, D.M. Ozonoff, Reproductive and developmental health effects of prenatal exposure to tetrachloroethylene-contaminated drinking water, Environ. Sci. Processes Impacts 22 (3) (2020) 555–566.
- [39] N. Guha, D. Loomis, Y. Grosse, B. Lauby-Secretan, F. El Ghissassi, V. Bouvard, L. Benbrahim-Tallaa, R. Baan, H. Mattock, K. Straif, Carcinogenicity of trichloroethylene, tetrachloroethylene, some other chlorinated solvents, and their metabolites, in, Elsevier, 2012.
- [40] I. Rusyn, W.A. Chiu, L.H. Lash, H. Kromhout, J. Hansen, K.Z. Guyton, Trichloroethylene: Mechanistic, epidemiologic and other supporting evidence of carcinogenic hazard, Pharmacol. Ther. 141 (2014) 55–68.
- [41] U.S. EPA, National primary drinking water regulations, in, 2021.
- [42] M.J. Moran, J.S. Zogorski, P.J. Squillace, Chlorinated solvents in groundwater of the United States, Environ. Sci. Technol. 41 (2007) 74-81.
- [43] C.G. Schreier, M. Reinhard, Catalytic hydrodehalogenation of chlorinated ethylenes using palladium and hydrogen for the treatment of contaminated water, Chemosphere 31 (1995) 3475–3487.
- [44] E. López, S. Ordóñez, F.V. Díez, Deactivation of a Pd/Al2O3 catalyst used in hydrodechlorination reactions: Influence of the nature of organochlorinated compound and hydrogen chloride, Appl. Catal. B 62 (2006) 57-65.
- [45] R. Navon, S. Eldad, K. Mackenzie, F.-D. Kopinke, Protection of palladium catalysts for hydrodechlorination of chlorinated organic compounds in wastewaters, Appl. Catal. B 119 (2012) 241-247.
- [46] D. Comandella, S. Woszidlo, A. Georgi, F.-D. Kopinke, K. Mackenzie, Efforts for long-term protection of palladium hydrodechlorination catalysts, Appl. Catal. B 186 (2016) 204-211
- [47] M.O. Nutt, J.B. Hughes, M.S. Wong, Designing Pd-on-Au bimetallic nanoparticle catalysts for trichloroethene hydrodechlorination, Environ. Sci. Technol. 39 (2005) 1346-1353.
- [48] M.O. Nutt, K.N. Heck, P. Alvarez, M.S. Wong, Improved Pd-on-Au bimetallic nanoparticle catalysts for aqueous-phase trichloroethene hydrodechlorination, Appl. Catal. B 69 (2006) 115–125.
- [49] B. Schrick, J.L. Blough, A.D. Jones, T.E. Mallouk, Hydrodechlorination of trichloroethylene to hydrocarbons using bimetallic nickelnanoparticles, Chem. Mater. 14 (2002) 5140-5147.
- [50] G. Yuan, M.A. Keane, Liquid phase hydrodechlorination of chlorophenols over Pd/C and Pd/Al<sub>2</sub>O<sub>3</sub>: a consideration of HCl/catalyst interactions and solution pH effects, Appl. Catal. B 52 (2004) 301–314.
- [51] G. Yuan, M.A. Keane, Role of base addition in the liquid-phase hydrodechlorination of 2, 4-dichlorophenol over Pd/Al2O3 and Pd/C, J. Catal. 225 (2004) 510-522.

- [52] M.I. Cobo, I.A. Conesa, C. Montes de Correa, The Effect of NaOH on the liquidphase hydrodechlorination of dioxins over Pd/ $\gamma$ -Al2O3, The J. Phys. Chem. A 112 (2008) 8715-8722.
- [53] S. Brunauer, P.H. Emmett, E. Teller, Adsorption of gases in multimolecular layers, J. Am. Chem. Soc. 60 (1938) 309-319.
- [54] E.P. Barrett, L.G. Joyner, P.P. Halenda, The determination of pore volume and area distributions in porous substances. I. Computations from nitrogen isotherms, J. Am. Chem. Soc. 73 (1951) 373-380.
- [55] C.A. Schneider, W.S. Rasband, K.W. Eliceiri, NIH Image to ImageJ: 25 years of image analysis, Nat. Methods 9 (2012) 671-675.
- [56] A. Kropf, J. Katsoudas, S. Chattopadhyay, T. Shibata, E. Lang, V. Zyryanov, B. Ravel, K. McIvor, K. Kemner, K. Scheckel, The new MRCAT (Sector 10) bending magnet beamline at the advanced photon source, in: AIP Conference Proceedings, American Institute of Physics, 2010, pp. 299-302.
- [57] T. Ressler, WinXAS: A new software package not only for the analysis of energy-dispersive XAS data, Le, J. Phys. IV 7 (1997).
- [58] D. Lin-Vien, N.B. Colthup, W.G. Fateley, J.G. Grasselli, The handbook of infrared and Raman characteristic frequencies of organic molecules, Elsevier, 1991.
- [59] R.M. Pasternack, S. Rivillon Amy, Y.J. Chabal, Attachment of 3-(aminopropyl) triethoxysilane on silicon oxide surfaces: dependence on temperature, Langmuir 24 (2008) 12963–12971.
- [60] N. Tillman, A. Ulman, J.S. Schildkraut, T.L. Penner, Incorporation of phenoxy groups in self-assembled monolayers of trichlorosilane derivatives. Effects on film thickness, wettability, and molecular orientation, J. Am. Chem. Soc. 110 (1988) 6136-6144.
- [61] J.J. Chruściel, M. Fejdyś, W. Fortuniak, Synthesis, characterization and microstructure of new liquid poly (methylhydrosiloxanes) containing branching units SiO4/2, Polymers 10 (2018) 484.
- [62] C. Tripp, M. Hair, Reaction of chloromethylsilanes with silica: a low-frequency infrared study, Langmuir 7 (1991) 923-927.
- [63] B.C. Smith, Infrared spectral interpretation: a systematic approach, CRC Press,
- [64] P.J. Launer, Infrared analysis of organosilicon compounds: spectra-structure correlations, Silicone Compounds Register Rev. 100 (1987).
- [65] A.L. Smith, Infrared spectra-structure correlations for organosilicon compounds, Spectrochim. Acta 16 (1960) 87-105.
- G. Camino, S. Lomakin, M. Lageard, Thermal polydimethylsiloxane degradation. Part 2. The degradation mechanisms, Polymer 43 (2002) 2011-
- K.L. Mittal, Silanes and Other Coupling Agents, CRC Press, 2020.
- [68] J. Coates, Interpretation of infrared spectra, a practical approach, Encyclopedia of analytical chemistry: applications, theory and instrumentation, (2006).
- [69] V.M. Litvinov, P.P. De, Spectroscopy of rubbers and rubbery materials, iSmithers Rapra Publishing (2002).
- [70] A.L. Smith, J. McHard, Spectroscopic techniques for identification of organosilicon compounds, Anal. Chem. 31 (1959) 1174-1179.
- [71] A. Zecchina, S. Bordiga, G. Spoto, L. Marchese, G. Petrini, G. Leofanti, M. Padovan, Silicalite characterization. 2. IR spectroscopy of the interaction of carbon monoxide with internal and external hydroxyl groups, J. Phys. Chem. 96 (12) (1992) 4991-4997.
- [72] B.A. Morrow, A.J. McFarlan, Infrared and gravimetric study of an aerosil and a precipitated silica using chemical and hydrogen/deuterium exchange probes, Langmuir 7 (8) (1991) 1695–1701.
- [73] G. Davidson, Spectroscopic properties of inorganic and organometallic compounds, Roy. Soc. Chem. (1993).
- [74] S.M. Iftiquar. Structural studies on semiconducting hydrogenated amorphous silicon oxide films, High Temperature Mater. Processes: An Int. Quart. High-Technol. Plasma Processes 6 (1) (2002) 19.
- [75] P.-Y. Mabboux, K.K. Gleason, Chemical bonding structure of low dielectric constant Si: O: C: H films characterized by solid-state NMR, J. Electrochem. Soc. 152 (1) (2005) F7.
- [76] I. Lisovskyy, V. Litovchenko, D. Mazunov, S. Kaschieva, J. Koprinarova, S. Dmitriev, Infrared spectroscopy study of Si-SiO<sub>2</sub> structures irradiated with high-energy electrons, J. Optoelectron. Adv. Mater 7 (2005) 325–328.
- I.P. Lisovskii, V.G. Litovchenko, V.G. Lozinskii, G.I. Steblovskii, IR spectroscopic
- investigation of SiO<sub>2</sub> film structure, Thin Solid Films 213 (2) (1992) 164–169. [78] R. Mariscal, M. López-Granados, J.L.G. Fierro, J.L. Sotelo, C. Martos, R. Van Grieken, Morphology and surface properties of Titania–Silica hydrophobic xerogels, Langmuir 16 (24) (2000) 9460–9467.
- [79] M. Thommes, K. Kaneko, A.V. Neimark, J.P. Olivier, F. Rodriguez-Reinoso, J. Rouquerol, K.S. Sing, Physisorption of gases, with special reference to the evaluation of surface area and pore size distribution (IUPAC Technical Report), Pure Appl. Chem. 87 (2015) 1051-1069.
- [80] R.D. Gonzalez, T. Lopez, R. Gomez, Sol-Gel preparation of supported metal catalysts, Catal. Today 35 (3) (1997) 293–317.
- R.P. Schwarzenbach, P.M. Gschwend, D.M. Imboden, Environmental organic chemistry, John Wiley & Sons, 2016.
- [82] G.C. Bond, Metal-catalysed reactions of hydrocarbons, Springer, 2005.
- [83] J. Miller, A. Kropf, Y. Zha, J. Regalbuto, L. Delannoy, C. Louis, E. Bus, J.A. van Bokhoven, The effect of gold particle size on AuAu bond length and reactivity toward oxygen in supported catalysts, J. Catal. 240 (2006) 222-234.
- [84] C.W. Lopes, J.L. Cerrillo, A.E. Palomares, F. Rey, G. Agostini, An in situ XAS study of the activation of precursor-dependent Pd nanoparticles, PCCP 20 (2018) 12700-12709.

- [85] M.A. Newton, R. Nicholls, J.B. Brazier, B.N. Nguyen, C.J. Mulligan, K. Hellgardt, E. M. Barreiro, H. Emerich, K.K.(. Hii, I. Snigireva, P.B.J. Thompson, Effect of retained chlorine in ENCAT™ 30 catalysts on the development of encapsulated Pd: insights from in situ Pd K, L3 and Cl K-edge XAS, Catal. Struct. React. 3 (4) (2017) 149–156.
- [86] K.N. Heck, B.G. Janesko, G.E. Scuseria, N.J. Halas, M.S. Wong, Observing metal-catalyzed chemical reactions in situ using surface-enhanced Raman spectroscopy on Pd— Au nanoshells, J. Am. Chem. Soc. 130 (2008) 16592–16600.
- [87] J. Andersin, P. Parkkinen, K. Honkala, Pd-catalyzed hydrodehalogenation of chlorinated olefins: Theoretical insights to the reaction mechanism, J. Catal. 290 (2012) 118–125.
- [88] M.H. Seo, S.M. Choi, J.K. Seo, S.H. Noh, W.B. Kim, B. Han, The graphenesupported palladium and palladium-yttrium nanoparticles for the oxygen reduction and ethanol oxidation reactions: Experimental measurement and computational validation, Appl. Catal. B 129 (2013) 163–171.